# Boundary Current Response in $Ba_{0.34}K_{0.64}Fe_2As_2$ Superconducting Single Crystal Probed by Non-Resonant Microwave Absorption Technique.

By

**Tshiwela Caroline Ramashitja**

Submitted in accordance with the requirements for

the degree of

**MASTER OF SCIENCE**

In the subject

**PHYSICS**

at the

UNIVERSITY OF SOUTH AFRICA

**SUPERVISOR: Prof. Vijaya Srinivasu Vallabhapurapu**

**CO-SUPERVISOR: Prof. Vaith Sankaran**

**June 2016**

## Declaration

I declare that **"Boundary Current Response in $Ba_{0.34}K_{0.64}Fe_2As_2$ Superconducting Single Crystal Probed by Non-Resonant Microwave Absorption technique**" is my own work and that all sources that have been used or quoted have been indicated and acknowledged by means of complete references.

Signature:..... Date:.....

(T.C Ramashitja)

## Dedication

I dedicate my dissertation work to my family, a special feeling of gratitude to my loving life partner T. Telekisa whose words of encouragement and push for tenacity ring in my ears. My brother Marius has always been my role model.

## Acknowledgements

- Firstly I would like to express my deepest gratitude to my Supervisor Pro V.V Srinivasu for his full support, encouragement, expert guidance and understanding throughout my research. Working in his astonishing group (STEM- Superconductivity Technology and Emerging Materials) has been a humbling opportunity for me.
- I will would like to thank the Unisa Physics department for their unwavering support. Right from the Cod prof Lekala, his team and all group members of the superconductivity Technology and Emerging materials (STEM).
- I am indebted to Dr. Jayashree for moral support.
- Thanks also go to my fellow graduates at Unisa physics department. Special thanks go to my numerous friends (Langu and victor) who helped me throughout this academic exploration.
- To NRF for financial support, am humble grateful.
- To Unisa, Grow your own Timber
- Finally I would like to thank my mother, and brothers for their unconditional love and support during the Last two years, I would not have been able to complete this thesis without their continuous love and encouragement.
- Above all, I am humbled and overwhelmed with God's love, blessings, protection and guidance in the course of this work and my entire life.

## Definition of terms used.

HTSC: High temperature superconductors

NRMA: Non-Resonant Microwave absorption

EPR: Electron paramagnetic resonance

BaK122: $Ba_{0.34}K_{0.64}Fe_2As_2$

## List of Figures.

**Abstract.**

Non-resonant microwave absorption (NRMA) in superconducting materials has become a new experimental technique to probe and understand superconducting materials. For example cuprate superconductors are well studied with this technique. At the same time the technique is also evolving. This technique (NRMA) has been used to study magnetic shielding effects/boundary current in $Ba_{0.34}K_{0.64}Fe_2As_2$ (BaK122) single crystals of iron pnictides superconducting sample measured at 9.4 GHz below $T_C$ (4.2K-32K). It has been observed that a small modulation field used in NRMA experiment yield the boundary current response. We have established that the boundary current response depends on both modulation amplitude and the temperature. At high modulation field amplitudes and temperatures close to $T_c$ the boundary current response gets suppressed and flux modulated response dominates. At low temperatures far away from $T_c$, only the boundary current response dominates.

## Table of contents.

# Chapter 1

## 1. Introduction

## 1.1 Overview on Superconductivity

Almost a century has passed since the discovery of Superconductivity which was discovered on 1911 by Heike Karmerlingh Onnes who was studying the resistance of solid mercury at cryogenic temperatures using the recently produced liquid helium as refrigerant; now hundreds of superconducting materials are known i.e. C60 based organic and other iron based superconductors. A material is said to be a superconductor when the DC electrical resistance becomes zero and when it expels magnetic flux, these properties are depicted below.

### 1.1.1 Zero electrical resistivity

Heike Karmerlingh Onnes investigated the low temperature electrical resistance of mercury which abruptly dropped to zero as temperature was lowered below 4.21 K [1], shown below in Fig. 1.

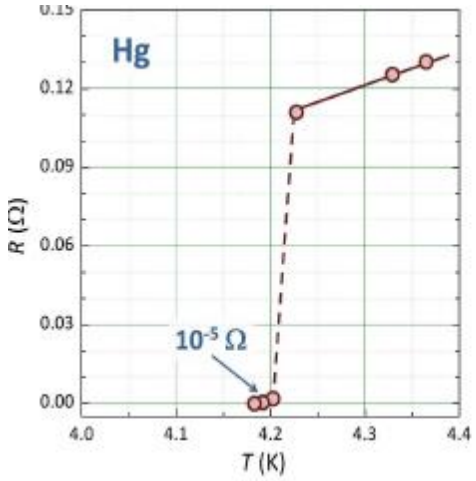


Fig.1.1 image taken from [2]: vanishing of electrical resistivity below a critical temperature $T_C$, discovered in mercury by Karmerlingh Onnes [1].

A material is said to be superconductor when DC electrical resistance becomes zero i.e. the resistance goes to zero as the superconductor is cooled below a characteristics temperature known as critical temperature (the temperature below which a material becomes superconducting) .There are important fundamentals and intuitively startling properties associated with superconductivity:

The transition from finite resistivity $\rho_n$ , in the normal state above a superconducting transition temperature $T_C$ , to $\rho = 0$ i.e. perfect DC conductivity $\sigma = \infty$ , below $T_c$ and the simultaneous change of magnetic susceptibility X from a small positive paramagnetic value above $T_C$ to X= -1 i.e. perfect diamagnetism below $T_C$ .

## 1.1.2 Meissner effect

When magnetic field is applied to superconductor, the magnetic field cannot penetrate inside the material therefore it create a current that screen out the magnetic field, it will expel the applied magnetic flux by a mechanism well known as the Meissner effect which is the next important discovery after the discovery of zero electrical resistivity[3].

The expulsion of the magnetic field originates a super current inside superconductor materials i.e. Inside a superconducting material there are paired electrons known as the cooper pairs, when they start to move they generate a current and this current will shield or protect the superconductor from the applied magnetic field, but however if the applied magnetic field is greater than the critical magnetic field, the field will penetrate in the form of flux and then the superconductor material will lose its superconductivity and then turns to normal state $B \neq 0$ .

It is important to recognize that the exclusion of the magnetic field inside a superconductor cannot be predicted by applying Maxwell's equation to a perfect conductor which has zero electrical resistance below certain $T_C$ , according to Maxwell's equation

$$\nabla \times E = -\frac{\partial B}{\partial t} \qquad (1.1)$$

The zero resistivity below $T_C$ leads to a constant B, so B will not change it is not zero; therefore the Meissner effect distinguishes a superconductor from a perfect conductor.

The superconducting state can be destroyed by an external magnetic field, the field $H_C$ is called critical field.

### 1.1.3 Types of Superconductors

Superconductors are divided into type I and type II according to their different behavior when placed under the influence of magnetic field. For a type-I superconductor as shown below in figure 1.2 (a), if the magnetic field is below $H_C$ , the material is in the superconducting sate; but as soon as the magnetic field is increased above $H_C$, which is different for different, the Meissner effect breaks down that is to say flux penetrates into the material then transit to normal state. But for type II superconductor, there are two critical fields; the lower critical fields $H_{C1}$ ($H_{C1}$ is the field at which first time flux enters into the superconductor sample), and the upper critical field $H_{C2}$, ($H_{C2}$ is the field at which a superconductor material turns normal. Below $H_{C1}$, the superconductor is in a pure superconducting state, the same as type I superconductor in magnetic field below $H_C$, which is called the Meissner state. But between $H_{C1}$ and $H_{C2}$, magnetic flux from external fields is no longer completely expelled, and the superconductor is in mixed state. Above $H_{C2}$, the superconductivity is completely destroyed and the material exists in a normal state as shown below in Fig. 1.2(b).

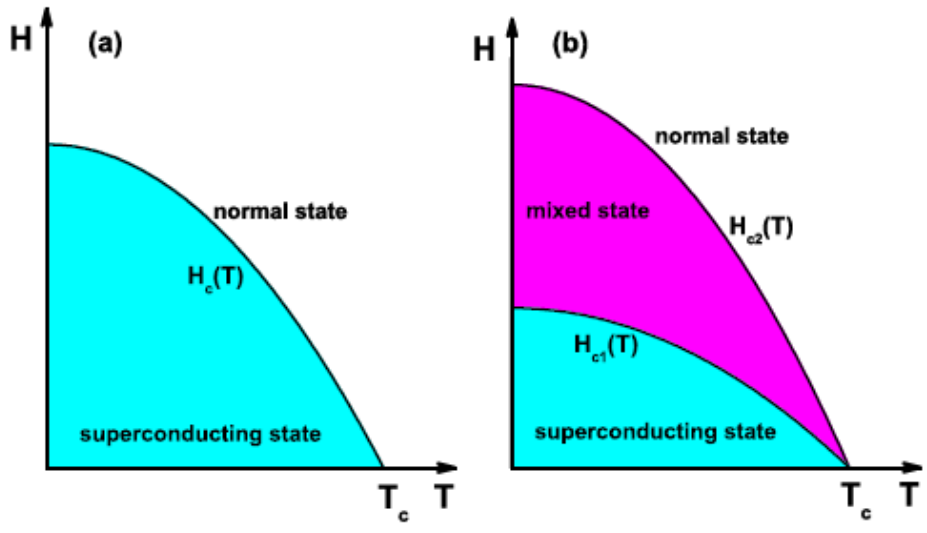

Fig.1.2 **(a**) Phase diagram for the behavior of type I a superconductor which switches abruptly from the Meissner state to the normal state at $H_C$, from the graph (b) type II superconductor shows a different behavior, at a lower critical field $H_{C1}$ the superconductor changes state from Meissner state with a complete screening to a state of vortex and finally at $H_{C2}$ to the normal state [4].

Type I: The superconductor switches abruptly over from the Meissner state to one of full penetration of magnetic flux, the normal state, at a well-defined critical field, $H_C$ . Examples of such materials are Hg, Al, and Sn. Fig. 1.2(a) shows a sketch of this behavior. Type II: The superconductor switches from the Meissner state to a state of partial penetration of magnetic flux, the mixed state, at a critical field $H_{C1}$. Thereafter it crosses over continuously to full flux penetration, the normal state, at the upper field $H_{C2}$. Examples: $Nb_3Sn$, NbTi, and all high $T_C$ cuprates. Fig. 1.2(b) shows this behavior.

Therefore when a superconductor is brought into a magnetic field, its behavior depends on the balance of its fundamental length scales, The first of these, the penetration depth $\lambda$ ($\lambda$ is the depth of penetration of magnetic flux from the surface of a superconductor) which is given by $\lambda = \sqrt{\dfrac{m}{4\mu_0 e^2 |\Psi_0|^2}}$ (1.2) where $\Psi_0$ is the equilibrium value of the order parameter in the absence of an electromagnetic field, and the coherence length $\xi$ which describes the shortest length over which the order parameter $\Psi$ can vary significantly, then it is given by

$$\xi = \sqrt{\frac{\hbar^2}{2m|\alpha|}} \qquad (1.3)$$

The ratio of these two length scales $k = \dfrac{\lambda}{\xi}$ determines the response of the superconductor to an applied magnetic field, where k is the Ginzburg-Landau parameter [5]. So when type II superconductor is put in a magnetic field, in a case where $H < H_{C1}$ , the average field B inside the specimen is zero which shows pure Meissner effect. When $H_{C1} < H < H_{C2}$ , the magnetic field penetrates inside specimen, the superconductor is divided into normal and

superconducting domains which are parallel to the external field. The normal domains are vortices, each with a radius of the $\xi$ and magnetic flux of $\phi_0$ . The density of the vortices increases with increasing external field until $H_{C2}$ , at which the distance between two vortices is about $\xi$ and the specimen transits from the superconducting to the normal state.

## 1.2 Magnetic properties of superconductors

High temperature superconductors have attracted features which are closely related to or have direct effect on non-resonant microwave absorption and radio frequency. Therefore in this section we intend to explain some of magnetic parameters and properties in relation to the electromagnetic dynamics of superconductors.

### 1.2.1 Critical state and critical currents

This brief discussion is done referring to [13], in the case of type II superconductors, density of defects fluxons are pinned by these defects and are held against the Lorentz force or the thermal force and move only through thermally activated process. Lorentz force arises due to the interaction of currents in the sample with fluxon. This can also be expressed as $F_L = J\Phi_0 \sin\theta$. When $\theta = 90^0$ the Lorentz force is maximum and $F_L = J\Phi_0$. Fluxon is held at the defect against this force till $F_L = J\Phi_0 = F_P$ where $F_P$ is the pinning force. If $F_L$ exceeds $F_P$ fluxons can move and an e.m.f arises which is in the direction of the current and leads to losses. The maximum loss less current that flow, (giving rise to the Lorentz force which is just equal to the pinning force and hence the fluxons are yet to move) is called the critical current. Any further increase of the current above this value will give rise to flux flow. (For the depinned fluxon state, the macroscopic critical current is zero even though thermodynamically the system has a condensate).

### 1.2.3 The Bean critical state model

The bean critical state model [27, 28] presents a meaning making explanation for the hysteretic magnetization of type-II superconductors in a temporally varying external magnetic field. For normal materials which have extremely thin filaments the magnetic field penetrates into the superconductors in the form of superconductive electron current vortices. The magnetization depends upon the vortex distribution for each of the magnetic vortices which carries the same amount of magnetic flux (one quantum). The assigning of vortices in

type-II superconductors according to the bean model is determined by the equilibrium between electromagnetic driving forces (Lorentz force) and forces pinning the vortices to material in homogeneities [27]. Magnetic vortices start to enter or leave the superconductor through its boundary whenever the external magnetic field is changed. The system of vortices rearranges itself into another meta-stable state such that all vortices are pinned again and the equilibrium with the external field at the boundary is re-established if a region appears where the driving forces overcome the pinning forces. The system more rapidly adjusts itself to the changing external conditions since the unpinned vortices move quickly, and thus a quasi-stationary model with instantaneous interaction is justified.

These are the basic and somewhat simplified assumptions of the phenomenological of the critical states models of hysteretic magnetization in type-II superconductors in terms of macroscopic quantities and maybe summarized by the statement that the current density never exceed some critical value determined by the density of pinning forces and thus, as long as this threshold is not reached, the magnetic induction, determined by the assigning of vortices, remains unchanged. In Bean model of critical states Jc, is a constant determined by the properties of superconductor material, which implies through the Maxwell equation that macroscopic current density is equal to the critical current Jc and is directed to normal fluxons and parallel to the boundary. This leads to the fluxons density decreasing linearly with distance from the boundary of the sample, which in turn gives characteristic magnetization (M) vs field (H) plot. however Kim et al.[29] found that generally the critical current density depends on the magnetic field and various relations of the type Jc =Jc(IHI) have been proposed [30, 31]. The Magnetization relations for a slab of thickness D is given as

$$-4\pi M = H - H^2 / 2H^* \text{ For } H \le H^* \quad (1.4)$$

$$-4\pi M = H^* / 2 \text{ For } H \ge H^* \quad (1.5)$$

In this case $H^* \equiv \pi J_C D / 5$ is the field value where the flux density reaches the centre of the slab. The value of $J_C$ can be calculated by determining the value of $H^*$ experimentally [27, 32, 33].

## 1.2.4 Anderson-Kim model

In the same year 1962, when Bean [27], introduce a critical state model for reporting the magnetization of a hard superconductor by assuming that the critical current density is

independent of magnetic field, Kim, Hempstead and Strnad [28] extended the Bean model by incorporating magnetic field dependence in the critical current density. However Kim model did not turn out as useful as Bean's model, in this case the studies based on Kim model remained limited mainly to the theoretical type of work in areas like the low field AC susceptibility [34-37] and fishtail effect [38].

There are two reasons which make the Kim model less usefulness and those reasons are stated below

(i) There's only one equation in this model which contain two constant $k$ and $H_0$, as shown below[39]

$$J_{C,Kim}(H) = k/(H_0 + H), \qquad (1.6)$$

In this case $J_{C,Kim}(H)$ is the critical current density in the Kim model, but a unique solution of $k$ and $H_0$ requires two equations between them.

(ii) The fact that for $H_0 = 0$ and $H = 0$ Eqn (1.6) leads to an infinite value, which is unphysically.

However it has been proven by various studies that using the hysteretic magnetization it is possible to get rid of the above two mentioned problems in favour of a consistent and practically useful version of the Kim model [39]. Furthermore the hysteretic Kim model has been applied to the Cuprate i.e. $YBa_2Cu_3O_7$, $Bi_2Sr_2CaCu_2O_{8+x}$ and iron based superconductors i.e. $Ba_{0.72}K_{0.28}Fe_2As_2$ practical usefulness.

## 1.2.5 Low critical magnetic field and high critical magnetic field

Just by considering the energetics of the system the lower critical field, $H_{C1}$, and the upper critical field $H_{C2}$ can be estimated. In a case of $H_{applied} = H_{C1}$, the field at the core of vortex will be $H_{C1}$ and then it will decrease to zero over the length $\lambda$. The flux will then be approximately $\pi\lambda^2 H_{C1}$ and this must be equal to the flux $\Phi_0$ hence $H_{C1} = \frac{\Phi_0}{\pi\lambda_1^2}$ upon subjecting a type II superconductor to a field higher than $H_{C1}$ the Meissner screening breaks down, individual flux quanta penetrate the superconductor. If $H_{applied} = H_{C2}$ the vortices are packed in tightly as they will go while maintaining the superconducting state, hence each will

take up an area approximately $\pi\xi^2 H_{C2}$, hence this will gives the estimate $H_{C2} \approx \frac{\Phi_0}{\pi\xi^2}$ [6]. When the applied field exceeds $H_{Cj1} = \frac{\Phi_0}{2\pi\lambda_j}(2\lambda_L + d)$[12] where d is the thickness of the barrier, fluxons entering the junction. These fields are very small compared to that of bulk $H_{C1}$

### 1.2.6 Weaklinks and Josephson junctions

Weaklinks can be established in several ways, one of the methods is a creation of typical dimensions like coherence length a long continues film of a single superconductor. This gives a Dayem bridge. Also very narrow interruption of superconducting properties can be achieved by depositing a high $T_C$ film across a naturally occurring grain boundary substrate. The grain boundary forces the superconductor to develop a chain of defects along the length of the grain boundary [9].

The Josephson Effect is the phenomenon of electric current passing between the two weakly coupled superconductors, separated by a very thin insulating barrier. This arrangement (two superconductors linked by a non-superconducting barrier) is known as Josephson junction; the current that crosses the barrier is the Josephson current. Macroscopic wave function $\Psi = \rho^{\frac{1}{2}} e^{i\theta}$ can describe superconductor as a whole and it is characterized by its amplitude $\rho = |\Psi^2|$ which is the density of cooper pairs and $\theta$ is the phase. For a number of pairs N, the phase is undefined due to the uncertainty $\Delta N \Delta\theta = 2\pi$, but if the phase is fixed at a point it is automatically fixed at all other points due to long range order.

When two different superconductors are separated by a thin insulator layer of dimension 10 $^0$A [6] their macroscopic wave function overlap to form a weak coupling. If the coupling energy is greater than the thermal energy then cooper pair s tunnel from one superconductor to the other with phase correlation or phase locking. The transport across the barrier is the tunneling process hence it explains the low current, in such a case these weakly coupled superconductors behave as single superconductor with $I = I_C \sin(\theta)$ (1.7)

Where $I_C$ is the critical current $\frac{\partial\theta}{\partial t} = \left(\frac{2e}{\hbar}\right)v$ (1.8)

And v is the voltage across the junction. Thus, even when no voltage V is applied across the junction the electric current can pass the barrier and its magnitude depends on the phase difference between the two superconductors, this is called the DC Josephson effect. The coupling energy is given by $E_j = -\frac{I_C\Phi_0}{2\pi}\cos\theta$ (1.9) where $V \neq 0$ across the junction;

the current $I = I_C \sin\left(\theta + \frac{2ev}{\hbar}\right)t$ (1.10)

Oscillates with an angular frequency $\omega = \frac{2eV}{\hbar}$, this is the AC Josephson effect [6].

### 1.2.7 Fluxon pinning

The following brief outline is obtained from ref [13], when magnetic field due to either an external applied field or electric current flowing through the superconductor exceeds $H_{C1}$, flux enters the superconductor (type II), in the form of fluxons, carrying single flux quanta $\Phi_0$.

Flux pinning arises in the following manner, at the defect, the condensation energy is reduced. Then the configuration namely the location of a flux line at the defect is energetically favorable, because now the flux line core has to provide only for the reduced condensation energy is a crude measure of the pinning strength.

$F_P = \frac{U_P}{\xi} = \xi^2 H^2 / 2\mu_0$ (1.11)

Here $U_P$ is the pinning energy. HTSC, the smallness of $\xi$ causes intrinsic pinning due to the discreetness of lattice itself. Flux line can also be held in its place when there is a strong interaction of the flux line with the rest of the flux lines. In this case with what force the entire flux lattice (or flux bundle) is pinned determines the $J_C$, the macroscopic (extrinsic) critical current. This extrinsic $J_C$ is orders of magnitude smaller than intrinsic depairing current that arises from the unbinding of cooper pair at high superfluid velocity.

### 1.2.8 Penetration Depth of Josephson junction.

In a superconductor without any weak links, magnetic field penetrates into the bulk of the superconductor to a depth equal to the London penetration depth $\lambda_L$ . However, in a superconductor such as high Tc oxides ceramic pellet, the magnetic field penetrates first into the Josephson Junctions, whose penetration depth is much larger than London penetration depth [6].

In response to weak magnetic field, $H_o << \Phi_o / (2\pi\lambda_j d)$ , the junction will set up screening currents given by equation 1.11 which corresponds to that in a bulk sample to stop field penetration.

$$H(x) = H_0 e^{(-x/\lambda)} \qquad (1.12)$$

The quantity $\lambda_j$ is referred to as the Josephson penetration depth and it epitomizes the depth of magnetic field penetration into the Josephson junction. It has dimensions of the length and can be expressed as 2.0[14]. It offers essential information in regards to solutions dynamic in long Josephson junctions (long Josephson junctions are junctions with one dimension larger than the Josephson depth [15].

$$\lambda_j = \left( \frac{\Phi_0}{2\pi\mu_0 j_C d} \right)^{\frac{1}{2}} \qquad (1.13)$$

In this case $\mu_0 = 4\pi \times 10^{-7} Hm^{-1}$ , $\Phi_0 = 2.07 \times 10^{-15} Wb,$ $j_C$ is the critical current density through the junction given in $Am^{-2}$ and d is expressed in m. For instance, niobium material has a value of $\approx 21\mu m$ [15].

### 1.2.9 Lower critical field of Josephson junction ($H_{C1j}$)

The expression of free energy of individual Josephson vortex in an infinite junction is given as $W_0 = \frac{4\Phi_0 j_C}{\pi c} \lambda_j \qquad (1.14)$

And when this junction is subjected to an external magnetic field $H_{0,}$ the Gibbs free energy of a Josephson vortex can be represented as

$$G_0 = W_0 - \Phi_0 H_0 / 4\pi \qquad (1.15)$$

When the applied external magnetic field is adequately weak, the Gibbs energy $G_0>0$ and the Josephson vortex will not enter the junction as it is energetically unfavorable. However, when the external field is equal to $H_{Cj1}$ Gibbs energy equals to zero and the vortex penetrates the junction. The $H_{Cj1}$ is the lower critical field of Josephson junction given as [14]

$$H_{C1j} = \frac{\Phi_o}{2\pi\lambda_j(2\lambda_L + d)} \qquad (1.16)$$

d is the thickness of the barrier [13]. These fields are very small compared to that of bulk $H_{C1}$

## 1.2.10 Surface impedance

Surface impedance measurement is one of the most indispensable ways of characterizing a superconductor material. Having the information of the complex wave at frequency $\omega$ can be determined [16]. For a superconductor occupying the half space, $z \geq 0,$ the microwave surface impedance is a ratio of electric field and magnetic field on the surface of a superconductor which is defined as

$$Z_s = R_s + iX_s = \frac{E_t(z=0)}{\int_0^\infty J_s(z)dz} \qquad 1.17$$

Where the $E_t$ (z=0) is the tangential electric field at the plane boundary of z=0, and $J_s$ is the surface current density flowing parallel to the plane boundary [17]. The surface impedance has a relationship with a complex wave number $(\beta)$ of a plane wave penetrating into the metal given as [18].

$$\beta = \omega\mu_0 / Z_s \qquad 1.18$$

In equation 1.17 the real part, $R_s$, and the imaginary part $X_s$, are called the surface resistance and surface reactance, respectively

$$R_S = \frac{1}{2}\omega^2 {\mu_0}^2 \sigma_n x_n \lambda_L^3 \qquad 1.19$$

$$X_S = \omega\mu_0\lambda_L \qquad 1.20$$

Where $\mu_0$ is the free–space permeability, $\omega$ is the angular frequency of the microwave radiation, $x_n$ is the fraction of the normal fluid, $\sigma_n$ is the normal state conductivity, and $\lambda_L$ is the temperature dependent London penetration depth [17].

According to the two fluids model the expression for $\sigma_n$ and $\lambda_L$ are given as [18],

$$x_n(T) = 1 - (\lambda_0^2 / \lambda_0^2) \qquad 1.21$$

$$\lambda_L(T) = \lambda_0 / \sqrt{1 - (T / T_C)^4} \qquad 1.22$$

From equation 1.19, important information on surface resistance can be obtained which is crucial in application of superconductors in passive microwave devices. Also, fundamental parameters such as London penetration depth can be extracted from equation 1.22 Furthermore, by knowing the surface resistance of a superconductor, microwave power dissipated can be expressed as

$$P = \frac{1}{2} RH^2 \qquad 1.23$$

This expression is invoked when dealing with low field microwave absorption measurement. Since the microwave power absorption obtained in a derivative form, the derivative of equation 1.23 is used [19].

$$\frac{dP}{dH} = \frac{d}{dH}\frac{1}{2} RH^2 \qquad 1.24$$

## 1.2.11 Fluxon Quantization

Detailed information about flux quantization is given in reference [20]. In a ceramic HTSC, magnetic field enters in the form of fluxons, and then some region of the superconductor is in the mixed state. Given the order parameter of a superconductor is

$$\psi = |\psi| e^{i\varphi} \qquad 1.25$$

The line integral of gradient $\Delta\varphi$ around a closed contour encircling the normal domain has to be given by $2\pi$, where $N \in Z$. Assuming that the order parameter is single valued at any

given point and $\int_1^2 dl\varphi = \varphi_1 - \varphi_2$ is independent of the path connecting the start and the end point, we have [20]

$$\oint dl.\nabla\varphi = 2\pi N \qquad 1.26$$

The gauge invariant phase of the order parameter now has the gradient

$$\nabla\varphi GI(r) = \Delta\varphi(r) - \frac{2e}{\hbar}A \qquad 1.27$$

Where A is a vector potential coupling the magnetic field to the superconducting order parameter and $2e$ is the charge of a cooper pair. Using the modification $2e/\hbar = 2\pi/(h/2e) = 2\pi\pi/\Phi_0$ and subjecting the gauge invariant order parameter to the constraint as shown $\oint dl\nabla\varphi GI = 2\pi N$ 1.28

Hence we obtain [20],

$$\frac{2\pi}{\Phi_0}\oint dl \times A = 2\pi N \qquad 1.29$$

Applying stokes theorem we obtain

$$\int_C dl \times A = \iint_S dS\nabla \times A = \iint_S dSB \equiv \Phi = N\Phi_0 \qquad 1.30$$

Where $B = \nabla \times A$ and $\Phi$ is the magnetic flux through the surface S enclosed by the contour C [20]. This flux is thus seen to be quantized in units of $\Phi_0 \approx 2.07 \times 10^{-15} Wb$

## 1.2.12 Josephson junction and Josephson Effect

When a superconductor is cooled below its transition temperature, the electrons condense forming a macroscopic quantum state. In this case, all electrons in the superconducting condensate are defined by a single complex wave function given as

$$\psi = |\psi|^{i\varphi} \qquad 1.31$$

Where $|\psi|$ is the magnitude of superconducting order parameter which is a measure of the density of superconducting electrons, whereas $\varphi$ is the phase connected to the flow of super currents [21]. As soon as two superconductors are weakly coupled together as shown in Fig.1.3**,** their superconducting order parameters overlap and consequently electrons flow. The junction formed is called Josephson junction and the nature of coupling determines the amount of current (2.19) flows between the two superconductors

$$I = I_C \sin\varphi \qquad 1.32$$

In this case $I_C$ is the critical current (the maximum current that a junction can accommodate before dissipation occurs)

When the voltage is applied across the junction, the phase varies according to the equation 1.33 It results to an AC Josephson effect.

$$\frac{d}{dt}\varphi = \frac{2eV}{\hbar} \qquad 1.33$$

The amplitude of the DC Josephson current in equation 1.32 depends on temperature. Ambegaokar and Baratoff derived an equation of the critical current for tunneling junction with conventional superconductors as [22]

$$I_C(T) = \frac{\pi\Delta(T)}{2eR_n}\tanh\frac{\Delta(T)}{2k_BT} \qquad 1.34$$

In this case $R_n$ ,is the junction resistance in the normal state and $\Delta(T)$ is the energy gap. The Josephson current is maximal at T=0

$$I_C = \frac{\pi\Delta(0)}{2eR_n} \qquad 1.35$$

Once $I > I_C$, a current of normal electrons will flow through the junction in addition to the supercurrent. This results to the formation of resistively shunted Josephson junction (RSJ). Capacitor connected parallel to one another and a normal resistance are considered as circuit made by the RSJ. The sum of normal current will be the total current of this circuit. V/R, current through capacitor is given by $C\frac{dv}{dt}$, and supercurrent $I_S = I_C \sin\varphi$ [22].

$$I = I_C \sin\varphi + \frac{V}{R} + C\frac{dV}{dt} \qquad 1.36$$

With some mathematical manipulation, equation 1.36 gives

$$\frac{I}{I_C} = \sin\varphi + \frac{d\varphi}{d\tau} + B_C \frac{d^2\varphi}{d\tau^2} \qquad 1.37$$

Here $\beta_C = 2\pi I_C R^2 C / \Phi_0$ is Stewart-McCumbers parameter.

The current–voltage, I-V characteristics can be described by Stewart-McCumbers parameter $\beta_C = 2\pi I_C R^2 C / \Phi_0$. In the limit $\beta << 1$, the 1-V dependence is non-hysteric (non-dissipative) and is given by $V(I) = R(I_s^2 - I_c^2)^{1/2}$ while when $\beta >> 1$ the junction becomes hysteretic (dissipative) [23]

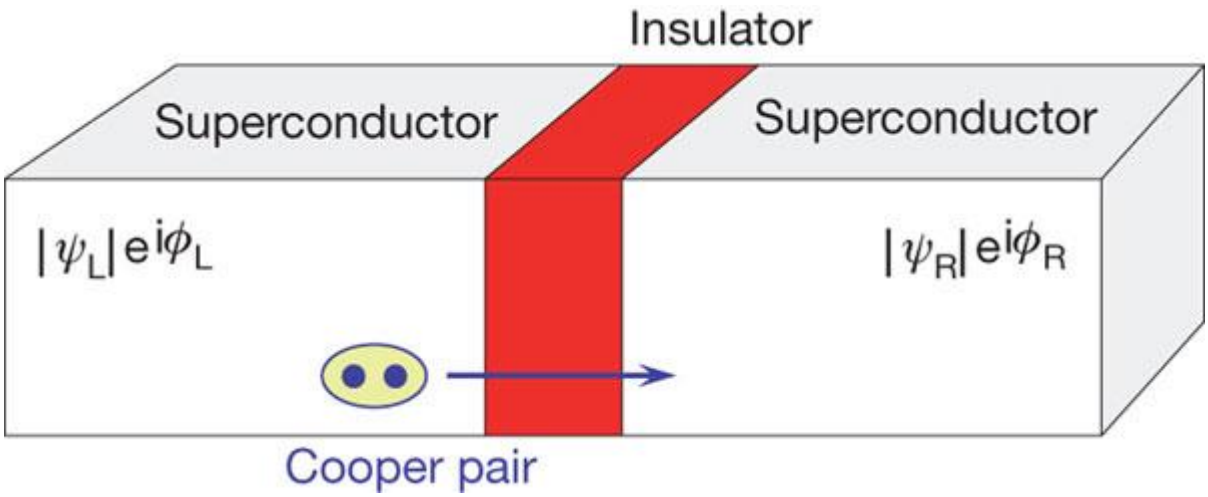


*Fig. 1.3: A schematic Josephson junction showing two superconductor separated by an insulating layer*.

Josephson junction results in any form of weak link in a superconductor where the critical current is significantly suppressed. They include SIS tunneling, SND sandwich, micro bridge formed by constriction, point contact junction and a small drop on a superconducting wire [22]. Inter-granular and intra-granular weak links are from Josephson junction in ceramic superconductors. Josephson junction may be formed within a unit cell as a result of sufficiently low inter-layer coupling in layered superconductor [24].

Josephson Effect has been employed in Josephson junction related applications such as SQUIDs and QUBIts. It's an achievement claim in the intrinsic Josephson junction (ijj). It employs the Josephson Effect in which direct current voltage is naturally converted into a high frequency electric current. The ijj shows potential in acting as a source of subterahertz and terahertz frequencies hence closing the famous terahertz gap [21].

### 1.2.13 Josephson coupling Energy

Josephson junctions' parameters have different values, which imply that, the idea of Tc ceramic superconductors being anisotropic in nature. One of these parameters is Josephson coupling energy $E_j$. This energy is associated with a macroscopic variable $\varphi$ i.e. the phase difference between two superconductors, which permits the transport of cooper pairs between superconducting electrons [25]. By considering two superconducting electrodes, the Josephson coupling energy is expressed as follows (grains) below Tc [25, 26]

$$E_j(T) = \frac{\hbar l_c}{2e} = \frac{h}{8e^2 R_n}\Delta(T)\tanh\left(\frac{\Delta(T)}{2K_B T}\right) \qquad 1.38$$

$I_c$ is the Josephson critical current between the grains, $R_n$ is the normal state resistance and $\Delta(T)$ is the BCS energy gap of the grains. Phase coherence exists at low temperature and magnetic field which results to maximum Josephson junction current. In this state the coupling is enhanced consequently $E_j$ is high and the junction acts as bulk.

## 1.3 Problem statement

The absorption of microwave and RF waves by high-Tc superconductors is very sensitive to very small applied field (0-100G), this phenomenon is well known as non-resonant microwave RF absorption [7]. This phenomenon is well studied in high-Tc cuprates [7], this experimental technique is very useful in understanding shielding currents, fluxon dynamics, quality of sample, identifying superconducting phases etc. [7]. Not many studies of this phenomenon are available in iron pnictides, in this thesis we shall study this phenomenon in iron pnictides.

The NRMA technique registers the field derivative of microwave loss in a superconducting sample as a function of applied magnetic fields, it has been established that a small modulating fields used in NRMA experiment yield only the boundary current response [8, 9], small modulation fields cannot move magnetic flux in and out, thus only the boundary current (shielding current) response is observed in NRMA signals [7].

However if the modulation field is strong enough to modulate the flux density inside the superconducting sample, the magnetic flux dependent loss dominates and boundary current (shielding current) will be suppressed. This is explained in more detail by Dulcic and Portis [8].In Josephson junction the field and temperature dependence of microwave loss is determined by the field and temperature dependence of critical currents ( $I_C$ ), this is because these are currents which shield the external magnetic fields applied to granular superconductor.

Therefore in this work, a systematic and detailed non resonant microwave absorption study on BaK122 has been carried out to elucidate the temperature, microwave power and field modulation amplitude dependent microwave loss. We are motivated by the fact that few works on low field microwave absorption in iron based superconductors are available hence the need to fill the gap. We have employed non resonant microwave absorption method to probe and extract fundamental features and characteristics of this material.

With recently discovered iron pnictides superconductors, more particularly BaKFeAs has caught the attention of many in the field of condensed matter physics because of the high critical fields, high critical density, relatively less anisotropy and high Tc. These qualities make it potential candidate for the aforementioned high magnetic field and electrical devices applications which have found places in medical, security and academic research fields.

Low field microwave absorption method has been used to probe fundamental properties and characteristics of high temperature superconductors hence it will be used in this research.

## 1.4 Research Objective.

To study the Boundary currents response in a $Ba_{0.34}K_{0.64}Fe_2As_2$ single crystals probed by Non-resonant microwave absorption technique.

## 1.5 References


1. Onnes, H.K.: The superconductivity of mercury. Leiden comm, 120b.1911.
2. Hykel, D.: These del Unersite de Grenoble 2011
3. Srinivasu, V.V.: Research space CSIR, available online 2009.
4. Zhao Sheng Wang, *Institute of physics, Chinese Academy of sciences, Beijing* 2006.
5. Forgan, E.M., Nuttall, W.J., Kealey, P.G., Johnson, S.T., Riseman, T.M., Nutley, M.P.: School of physics and astronomy university of Birmingham BIs 2TT, UK (may 26 2003).
6. Srinivasu, V.V.: Non-Resonant rf and microwave absorption studies (PhD thesis) Indian Institute of science, India 1994.
7. Srinivasu, V.V., and Sastry, M.D.: *Applied superconductivity* Vol 4, No4 pp195-201 1996.
8. Dulcic, A., Rakvin, B. And Pozek, M.: Europhys. Lett. **10**, 593, 1989.
9. Portis, A.M., Blazey, K.W., Muller K.A., and Bednorz, J.G. Europhys.Lett, **5**,467 1988.
10. Fossheim, K.:*Superconductivity* 123-124, 2004
11. Josephson, B.D.: *Phys. Lett.*, **1**:251, 1962.
12. Lynn, J. W.: High Temperature Superconductivity, 11-12 1990.
13. Morgenstern, I.: In earlier and recent aspect of superconductivity edited Bednorz, J.G., and Muller, K.A.: Springer-verlag 291 1990.
14. Muller, P., and Ustinov A.V., Tinkham, M.: *Phys.Rev* B**47** 470 1993.
15. Franz, A., Wallraff, A., and Ustinov, A.V.: *J. Appl. Phys* **89** 471 2001
16. Gallop, J.C., and Radcliffe, W.J.: *Supercond. Sci. Technol***. 4** 568 1991.
17. Wu, C.J., and Chen, Y.L.: *Prog. Electromagn. Res* **111** 433 2011.
18. Aly, A.H., and Sabra, W.: Physica C **495** 126 2013.
19. Tripathy, M.R., and Srivastava, G.P.: *IEEE. Trans. Magn* **35** 4079 1999.
20. Fossheim, K., and Sudbo, A.: *Superconductivity physics and applications, Wiley, Chichester west Sussex, England*. 2014.
21. Welp, U., Kadowaki, K., and Kleiner, R.: Nat. Photonics **7** 702 2013.
22. Mourachkine, A.: *Room temperature superconductivity CISP, Chippenham, England*. 2004.

23. Nikolay Plakida. *High temperature cuprate superconductors experiment, theory and applications springer, Dubna Moscow Region, Russia.* 2010.
24. Moll, P.J.W., Zhu, X., Cheng, P., Wen, H.H and Batlogg, B.: Nat. phys. DOI: 10.1038/NPHYS3034. 2014.
25. Alvarez, G.A Iguchi, I., Wang, X.L Dou, S.X., and Q.W. J. *Appl.Phys.* **99** 08M514. 2006.
26. Srivastava, K.N.: *Superconductivity, theoretical and experimental aspect*, USA. 1996.
27. Bean, C.P.: Magnetization of high field superconductors. Rev. Mod. Phys. **36**, 31-39 1964.
28. De Gennes, P.G.: Superconductivity of metals and alloys Benjamin. 1966.
29. Kim, Y.B., Hempstead, C.F., and Strnad, A.R.: Phys, Rev, Lett. **9,** 306 1962; Phys, Rev, 129,528 1963.
30. Wang, J., and Sayer, M.: Physica C **212**, 395 1993.
31. Chen, J.L., and Yang, T.J.: Physica C **224**,345 1994.
32. Huebener, R.P.: in magnetic flux structures superconductivity, Springer series, solid state Sci Vol 6 1979.
33. Bean, C.P.: Rev of Mod. Phys **36** 31 1964.
34. Chen, D.X., Sanchez, A. : J Appl. Phys 70 5463 1991.
35. Chen, D.X., Sanchez, A., Puig, T., Martinez, L.M., and Munoz, J.S.: Physica C **168** 652 1990.
36. Chen, D.X., Mei, Y., and Luo, H.L.: Physica C **167** 317 1990.
37. Ravi, S., and Seshubai, V.: Phys. Rev B **49** 13082 1994.
38. Johansen, T.H., Koblischka, M.R., Bratsberg, H. And Hetland, P.O.: Phys Rev. B **56** 11273 1997.
39. Lal, R.: Physica C **470** 281 2010.

# CHAPTER 2

## 2. High temperature Superconductors

## 2.1 Cuprates

The identification of high temperature superconductivity in the Cuprate $La_{2-x}Ba_xCuO_4$ by Bednorz J.G and Muller K.A [1] at 35K,has come as a shock since many scientist claim that BCS mechanism could not produce transition temperatures higher than the McMillan limit(~39K) this was then put to rest in 1986, thus encouraging the generation of high temperature superconductivity. Wu et al [2] have affirmed superconductivity in YBCO with $T_C$ of 92K. It was established that the $T_C$ in this material is dependent on oxygen content.

Maeda et al [3] in 1988 has found that Ba-Sr-Ca-Cu-O (BSCCO) was superconducting at 110 K and following the same year a $T_C$ of 120 K in TI-Ba-Ca-O [4] was discovered by Sheng and Hermann. Other findings were made during 1993 in Hg-Ba-Cu-O system where it was shown that this material had a $T_C$ of 94 K [5]. In quick subsequence it was found that the Tc of this very material on applying pressure it increases up to 153 K [6].

Still today the cuprates YBCO and BSCCO are the most arguably best studied and explored copper-oxide superconductors and have more than 100 000 research papers devoted to them. These materials have supported in concede and understanding fundamental and principles and mechanism of superconductivity both in convectional and unconventional level.

Despite the efforts the main problems are still unresolved; there is a lack in understanding the origin and the nature of the different phases, the microscopic mechanism of the superconductivity is still unknown, furthermore these materials have believable restriction inherent in them such as anisotropy [8], short coherence length [7] and weak links [9], these materials have found places in fabrication of devices.

### 2.1.1 Different phases of cuprates

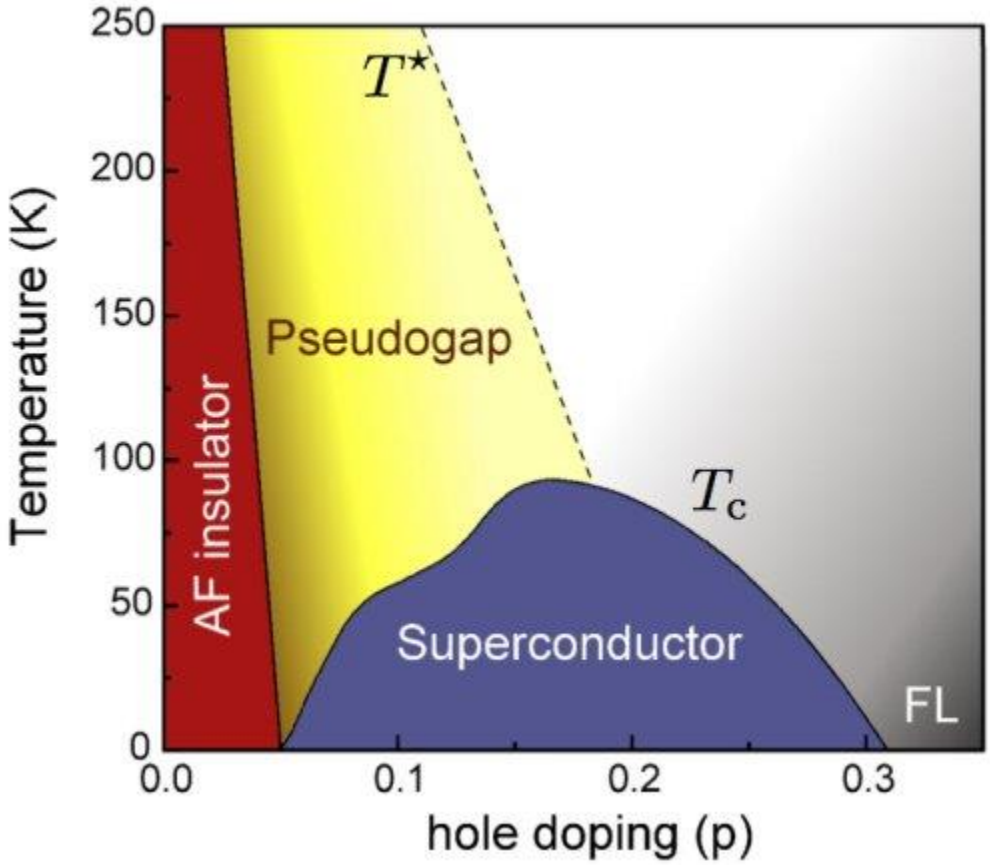


Figure 2.1 image taken from ref [10] shows the generic phase diagram of hole doping Cuprate materials.

(i) Mott insulator: the cuprates are poor conductors without doping

(ii) Pseudogap: when doped the Cuprate losses its antiferromagnetic ordering.

(iii) Superconductor: Increasing the doping in the Pseudogap state leads eventually to the SC (unless the temperature is too high.) $T_c$ becomes higher and higher until it reaches maximum (optimal doping) and then starts decreasing

## 2.1.2 Crystal Structure of Cuprates.

The following brief discussion is taken from [11]. The structure of high-$T_c$ copper oxide or Cuprate superconductors are often closely related to perovskite structure and the structure of these compounds has been described as a distorted, oxygen deficient multi-layered perovskite structure. One of the properties of the crystal structure of oxide superconductors is an alternating multi-layer of $CuO_2$ planes with superconductivity taking place between these layers. The higher the Tc, the more layers of $CuO_2$.This structure causes a large anisotropy in normal conducting and superconducting properties, since electrical currents are carried by holes induced in the oxygen sites of the $CuO_2$ sheets. The electrical conduction is highly anisotropic, with a much higher conductivity parallel to the $CuO_2$ plane than in the perpendicular direction. Generally, critical temperatures depend on the chemical compositions, cations substitutions and oxygen content. They can be classified as a super stripe that is particular realizations of super lattices at atomic limit made of superconducting atomic layers, wires, and dots separated by spacer layers that gives multiband and multi gap superconductivity.

Figure 2.2 shows a crystal structures of four cuprates, **A** the unit cells (total number of atoms, individual versus pairs of $CuO_2$ sheets, *c*-axis dimensions, etc.), most prevalent disorder types, and structural symmetry of these four cuprates differ considerably for Hg1201, YBCO, and Tl2201, the hole concentration in the $CuO_2$ sheets is altered by varying the density of interstitial oxygen atoms (each interstitial oxygen introduces up to two holes into nearby $CuO_2$ sheets), whereas in LSCO holes are introduced by replacing $La^{3+}$ with $Sr^{2+}$ ($p = x$ in this case). Hg1201 has a particularly simple crystal structure. It is the first member of the Ruddlesden–Popper family $HgBa_2CuCa_{n-1}Cu_nO_{2n+2+\delta}$, features one $CuO_2$ sheet per formula unit ($n$ =1), and the highest optimal $T_c$ ($T_c^{max}$ = 98 K) of all such single-layer compounds [e.g., $T_c^{max}$ = 39 K and 93 K for LSCO and Tl2201, respectively [12]. Furthermore, the physical properties of Hg1201 appear to be least affected by disorder, **B** the universal building block of the high-$T_c$ cuprates is the $CuO_2$ sheet. The most important electronic orbitals, Cu $d_{x^2-y^2}$ and O $p_\sigma$, are shown.

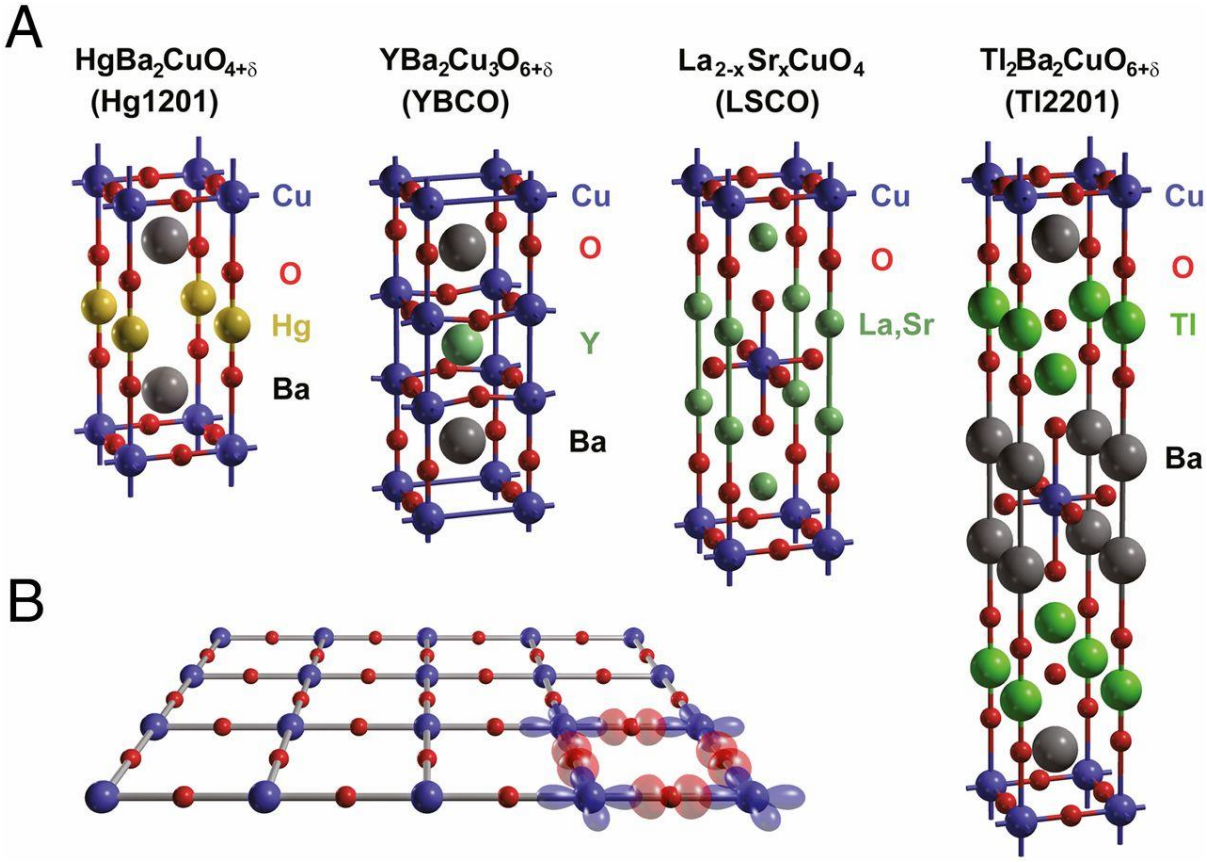


Figure 2.2 shows a crystal structure of four Cuprate superconductors [13].

## 2.2 Iron based superconductors

The discovery of superconductivity in iron-pnictides [14-15] has generated much interest. The parent compound consist of an iron pnictides layer that support superconducting currents interlaced with charge reservoir layer, this charge layer can be rare earth oxide or fluoride/alkaline earth fluoride, alkaline earth metal that give rise to a "1111" system, "122" system [15].The most interesting features of this class of iron pnictides is related to its magnetic and electronic properties. The parent compounds of both the ReFeAsO system and the $BaFe_2As_2$ system show a structural anomaly around 150~200K during the neutron scattering measurements, below which spin density wave (SDW), antiferromagnetic (AFM) ordering appears [16]. Amongst the families of the iron pnictides so far the most explored system is the "122" family, due to the simplicity of their crystal structure and availability of high quality single crystals. Superconductivity in the "122" compounds can be induced by doping with many materials, since recent scientist [ Seren et al.., 2009 ] showed that un doped parent compounds of iron pnictides exhibit a spin density wave antiferromagnetic order and it undergoes a structural phase transition from tetragonal to orthorhombic crystal symmetry upon cooling hence increasing the doping concentration the antiferromagnetic order is suppressed and a superconducting phase appears unlike the cuprates which the superconductivity is extremely sensitive to doping the Cu-O planes in the "122" pnictides superconductivity has been realized by changing each of the three constituents [17,18,19].The theoretical work has explained why the electronic structures of iron pnictides are susceptible to superconductivity via both hole and electron doping [20].

After the superconductivity in mercury at 4K by Karmerlingh Onnes in 1911, the search for new superconducting materials led to a slow increase of the highest known transition temperature $T_C$ over the decades, reaching a plateau at 23K with the discovery of the superconductivity of $Nb_3Ge$ by Gavaler [21], and the field was considered by many to be dead end. Until 1986, physicist had believed that BCS theory forbade superconductivity at temperatures above about 30K. In that year, IBM researchers Karl Muller and Johannes Bednorz searched for superconductivity in a new class of oxide materials and discovered superconductivity in LaBaCuO which had a transition temperature of 35K[22], for the discovery of new type of superconductivity they were awarded the Nobel prize in physics in 1987. The following year, liquid nitrogen temperature barrier 77K was broken with the discovery of $YBa_2Cu_3O_{7-x}$ [23], being superconducting at 93 K. soon a whole host of related

materials were found , and the Tc was risen to 138K at ambient pressure[24] and 164K under high pressure[25] as shown below the figure 2.3. Since a copper –oxide ($CuO_2$) plane is the common element in all these new high temperature superconductors these materials are referred to as the "Cuprates".

.

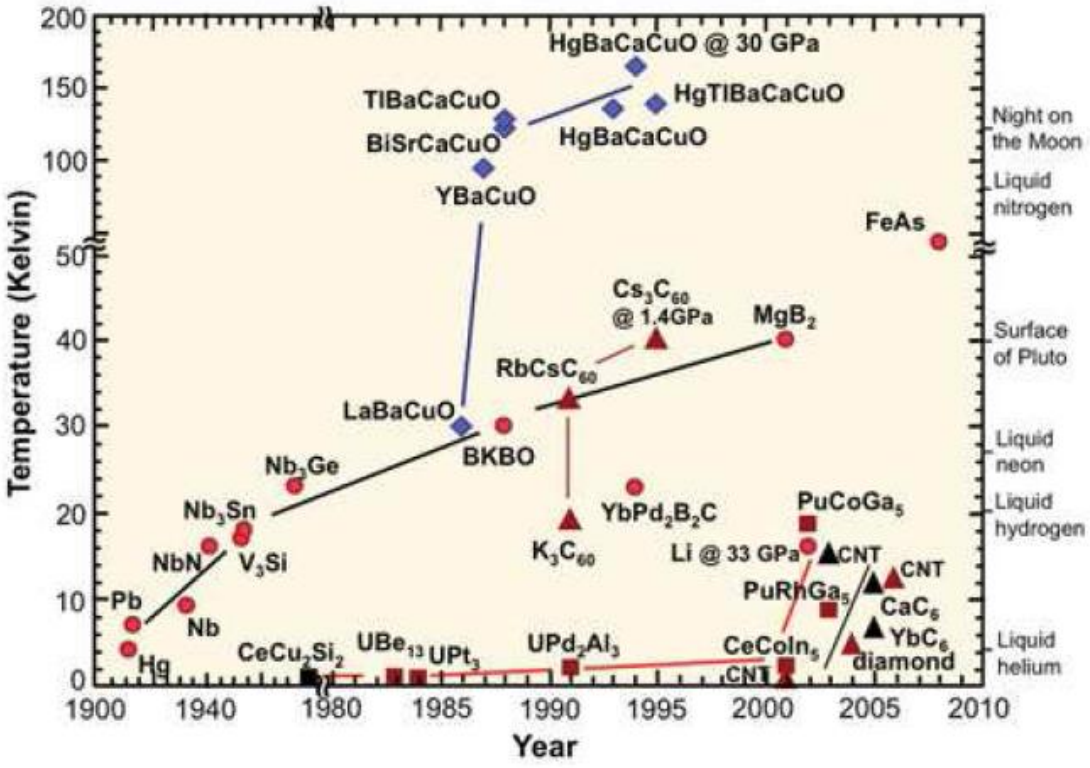


Figure 2.3 Evolution of critical temperatures of superconducting materials with time [26].

The identification of superconductivity in the cuprates was surprising and exciting, only simply because of the large increase in Tc, but also because no previous oxide superconductors had ever been found. Furthermore in their stoichiometric form (with no additional oxygen or other dopant atoms added), these materials are antiferromagnetic mot insulators. It is commonly accepted that magnetism cannot coexist with superconductivity. For example, Abrisokov and Gorkov showed that magnetic impurities disrupt superconductivity and depress Tc [27].

### 2.2.1 Different families of iron pnictides

Iron pnictides are grouped into four main families according to stoichiometric ratios of chemical constituents, namely 1111, 122, 111 and 11 types; their structures are presented on figure 2.4.

### (a)1111 family

The discovery of high-$T_C$ superconductivity in LaFeAsO1−xFx, increased by exchanging lanthanum with rare earth ions of smaller atomic radii in LnFeAsO and appropriate carrier doping or creating oxygen deficiencies, until it reached a maximum value of ~56 K until now in Gd1−xThxFeAsO [28]. This LnFeAsO came to be known as 1111 family. Other remarkable compounds showing a high superconductivity which came to be known are (i) SmFeAsO1−xFx ($T_C \approx$ 43K) [29], (ii) CeFeAsO1−xFx ($T_C \approx$ 41K) [30], (iii) NdFeAsO1−xFx ($T_C \approx$ 51K), and (iv) PrFeAsO1−xFx ( $T_C \approx$52K) [31].

### (b) 122 family

M. Rotter et al. [32] suggested $BaFe_2As_2$ as a potential new parent compound based on the similarities between $BaFe_2As_2$ and LaFeAsO. In fact, both compounds contain identical (FeAs) layers, and have the same charge accordance as follows: $Ba^{2+}$ $[(FeAs)-]_2$ vs. $(LaO)^+$ , $(FeAs)^-$.Partial replacement of Barium with Potassium (hole doping) induced superconductivity at 38 K in $Ba_{0.6}K_{0.4}Fe_2As_2$ [18], the first member of a new family of superconducting iron arsenide's known as the 122 family. This discovery was followed by reports of similar compounds with: (i) strontium ($T_C \approx$ 37K) [33, 34], (ii) calcium ($T_C \approx$ 20K) [35], and (iii) europium ($T_C \approx$ 32K) [36]. Later electron doping in $BaFe_2As_2$ by the partial replacement of Fe with Co with $T_C \approx$ 22K was reported by Sefat et al. [37].

### (c) 111 family

Superconductivity with $T_C$ up to 18 K was found and reported by Wang, X.C. et al. [38] in iron arsenide system LiFeAs (111).

### (d) 11 family

11 family was reported by F.-C. Hsu et al. [39], he observed superconductivity with zero resistance transition temperature at 8 K in the PbO-type αFeSe compound. Although FeSe has been studied quite extensively, a key observation is that the clean superconducting phase exists only in those samples prepared with intentional Se deficiency.

## 2.2.2 Structural properties

All structures of iron based superconductors share a common layered structure based upon a planar layer of iron atoms joined by tetrahedral coordinated pnictogen (P, As) or chalogen(S,Se,Te) anions arranged in a stacked sequence separated by alkali, alkaline earth metal or rare earth element. Now it is widely thought that the interaction that leads to the high-temperature superconductivity originates within these common iron layers, similar in nature to the common copper-oxide building block found in the cuprate high-temperature superconductors [40].

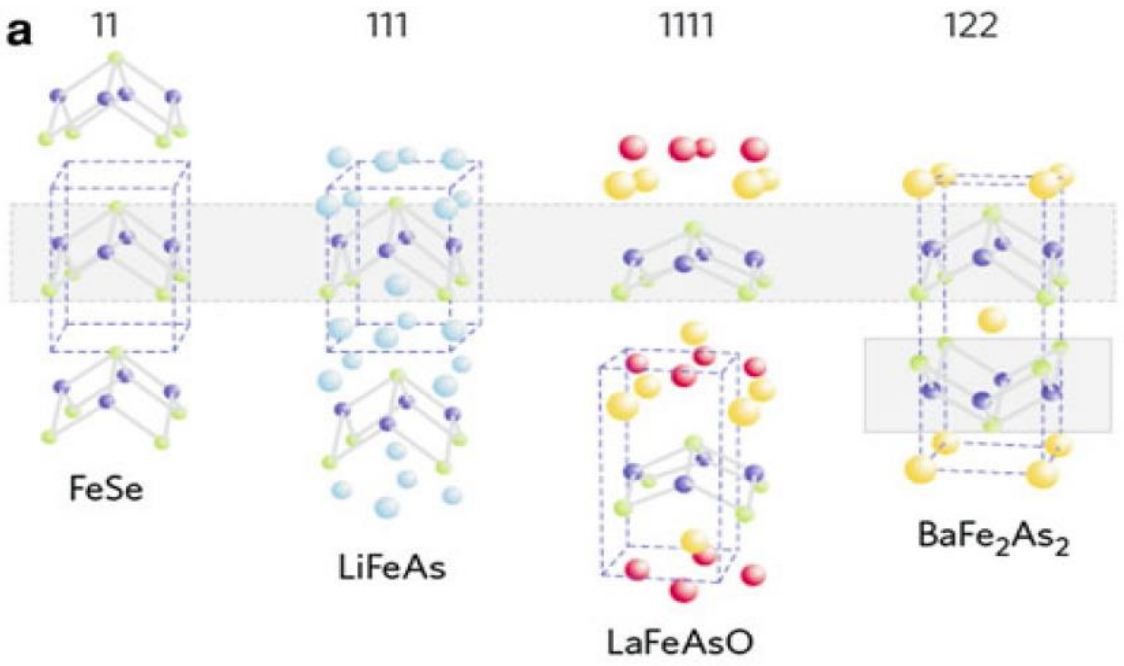


Figure 2.4 shows a Crystal structure of iron-based superconductor's classes [41].

All structures of iron based superconductors share a common layered structure based upon a planar layer of iron atoms joined by tetrahedral coordinated pnictogen ( P, As) or chalogen(S, Se, Te) anions arranged in a stacked sequence separated alkali, alkaline earth or rare-earth

and oxygen /fluorine "blocking layers ". Now it is widely thought that the interaction that leads to the high temperature superconductivity originates within these common iron layers, similar in nature to the common copper –oxide building block found in the cuprate high temperature superconductors [40].

As the temperature lowers, most of the undoped iron based compounds show a tetragonal-orthorhombic structural phase transition accompanied simultaneously or followed by an antiferromagnetic (AFM) transition (probably spin density wave type) , similar to the cuprates superconductors[38], as shown in figure 2.5 below and figure 2.1. However they are poor metals rather than Mott insulators and have five bands at the Fermi surface rather than one. As in the cuprates, chemical substitution also plays a key role in inducing the superconducting phase in iron –based superconductors.

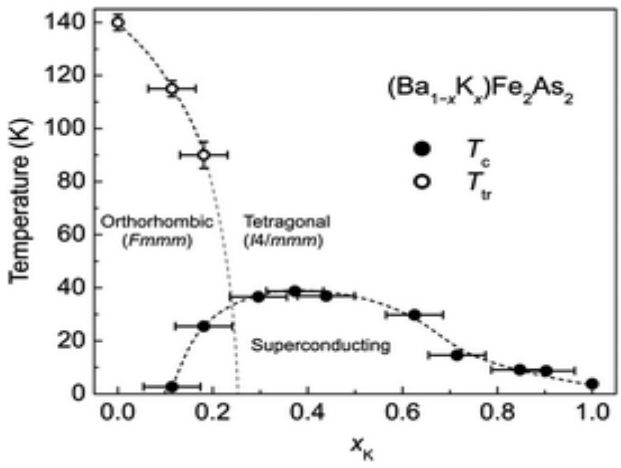


Figure 2.5 shows a structural phase diagram of $Ba_{1-x}K_xFe_2As_2$ [42].with a superconducting $T_c$ and the phase transition $T_r$ temperatures.

## 2.2.3 Phase diagram

The phase diagram of all iron based materials shows much common appearance in structural, magnetic and superconductivity phases hence can therefore provide a better way towards understanding the nature of superconductivity. Many scientist have make attempts to understand the phase diagram of iron based superconductors. The parent compound is semimetal at room temperature and exhibit anti ferromagnetic spin density wave phase transition at lower temperatures. Inducing superconductivity and suppressing long range of antiferromagnetic order in iron based compounds is done in three main methods; aliovalent

substitution i.e. doping the parent compound with potassium K or Cobalt Co ($Ba_{1-x}K_xFe_2As_2$, or Ba $(Fe_{1-x}Co_x)_2As_2$ as shown in Figure 2.6, isovalent substitution, that is modification of the crystallographic structure e.g. $BaFe_2(As_{1-x}P_x)_2$, $Ba(Fe_{1-x}Ru_x)_2As_2$ and lastly the application of external pressure. All those three methods have been found to yield very similar results that are suppression of long range antiferromagnetic order with successive induction of superconductivity characteristic dome-shaped region of the phase diagram [43, 44]. An increase of external pressure in certain materials leads to re-entrant superconducting phase with higher $T_c$ [45]. In figure 6 the phase diagram is showing the overlapping antiferromagnetic and superconducting regions of iron based compounds, the issue of the phase separation has been a topic of intense debate. It was given credence that some materials at the bright of iron pnictides research such as Ba $(Fe_{1-x}Co_x)_2As_2$ show microscopic coexistence of antiferromagnetic and superconductivity [46], where as other materials such as $Ba_{1-x}(K_xFe_2As_2)$, undergo intrinsic phase separation [47]. Single crystals $Ba_{1-x}(K_xFe_2As_2)$, $Ba(Fe_{1-x}Ru_x)_2As_2$ of sufficiently high quality has emerged in the recent experimental evidence in favour of microscopic phase coexistence [48-49], proving that in 122 iron pnictides the phase separation is an extrinsic effect. It has been made possible to study the properties of one via the other given that both phases coexist microscopically and homogeneously throughout the bulk of the crystal.

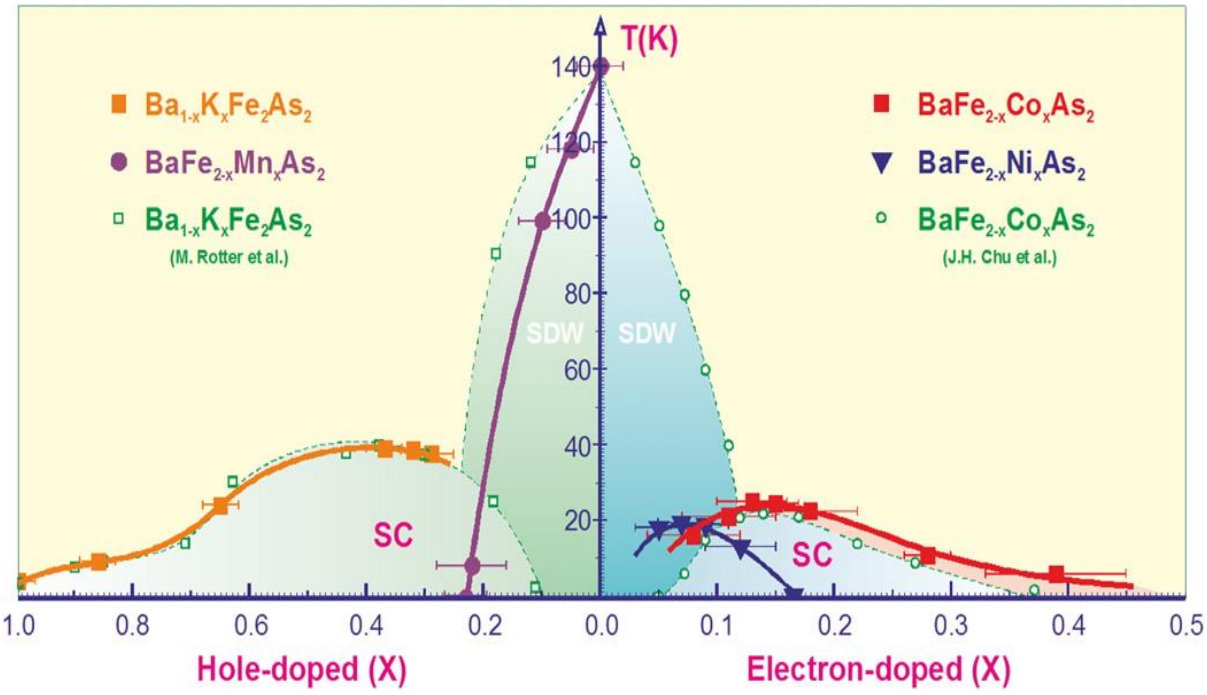


Figure 2.6 show a phase diagram of electron and hole-doped single crystals. The dashed lines in the left panel correspond to the phase diagram of polycrystalline samples from Rotter et al. [50], while those in the right panel are from single crystals and are reproduced from Chu et al [51].

### 2.2.4 Superconducting parameters of iron based Superconductors.

Iron-based superconductors have been studied extensively for both theoretical and practical reasons. There has been a lot of progress regarding the growth of this material especially the single crystal which has brought many achievements, which are helping in developing our physical understanding and also providing hope to finally solve the secret of high temperature superconductivity. Many important superconductivity properties are still a mystery, however some of the properties have been studied and made known to the world of scientist that our very own iron based superconductors has weak anisotropy [52,53], high current density [54, 55], relatively high Tc[56, 57], and high upper critical field [58, 59]

**Table 1** shows important superconducting state properties (Tc, upper critical field $\mu_0 H_{C2}$, coherence $\xi$, penetration depth $\lambda$ and Ginzburg number Gi) of iron based superconductors compounds representative of 1111, 122,111 and 11 families, YBCO and MgB2.It is indicated from the table that Tc of iron based superconductors is very low when compared to the Tc of

YBCO. However, the critical fields of iron based superconductors seem to be higher than that for $MgB_2$ and almost comparable to YBCO.

The YBCO system has a slightly higher anisotropy and Ginzburg number when compared to the 122 iron based superconductors. This is the evidence that pinning is stronger in iron based superconductors which results to reduce effect of thermal fluctuations [59]. This fact is has been proven in $SmFeAsO_{1-x}F_x$ which has stronger pinning potential than YBCO [60].

**Table 1** Important Superconducting state parameters of the FeSC families [61, 62] YBCO [63-66] and $MgB_2$ [67, 68].

| | **1111** | **122** | **11** | **YBCO** | **$MgB_2$** |
|---|---|---|---|---|---|
| Tc[K] | 55 | 38 | 16 | 93 | 39 |
| $Bc_2(T=0)[T]$ | >50 | 60 | 55 | >50 | 30 |
| $\gamma H$ | 5 | 2 | 2-3 | 4-14 | $3-5$ |
| $\xi_{ab}[nm]$ | 2.5 | 3 | 1.5 | 2.2 | 10 |
| $\xi_c[nm]$ | 0.6 | 1.5 | 0.6 | 0.4 | 2 |
| $\lambda_{ab}[nm]$ | 200 | 200 | 500 | 120 | 50 |
| Ginzburg $G_i$ number | $4\times10^{-4}$ | 1.5 $\times10^{-5}$ | $1\times10^{-3}$ | $5\times10^{-4}$ | $10^{-5}$ |

Critical current density and current anisotropy values for both single crystals and thin films of iron based superconductors, YBCO and $MgB_2$ [60] has been listed on **table 2**. It is noticeable

that the Jc for single crystals for YBCO compares well with that of 111, 11 superconductor and as well as that of 122 are of same order with $MgB_2$, on the contrary the Jc of thin films of 1111 superconductors is of significance less than that of YBCO, a fact accredited to the complex chemical composition of making 1111 films [69].

Refreshingly, Jc anisotropy which is elucidated as the ratio between the current flow in plane and out of plane ($J_C^{(ab)}/J_C^{(c)}$) is around 2 in all iron-based superconductors which are much alike the anisotropy in $MgB_2$ and much lower than the values of up to 30-50 found in cuprates. It then reveal unlike cuprates, iron based superconductors does not need complex elaborating processes for the fabrication of wires and tapes [60].

**Table 2** Indicates values of $J_C(0)$ for various superconductors.

| | 1111 | 122 | 11 | YBCO | $MgB_2$ |
|---|---|---|---|---|---|
| Single crystals | | | | | |
| $J_C(0)$ at 5K(A/cm) | $2\times10^6$ [70,71] | $3\times10^5$ [72,73] | $10^5$[74] | $3\times10^6$ [75] | $10^5$[76] |
| $J_C^{ab}/J_C^c$ | 2.5[71] | 2[77] | | 10-50[78,79] | 1-2 |
| $J_C(5)/J_C(0)$ | 0.8[71] | 0.5[73] | 0.3[74] | 0.5[75] | <0.01 |
| Thin films | | | | | |
| $J_C(0)$ at 5K($A/cm^2$) | $10^4$[80] | $4\times10^6$ [81,82,83] | $7\times10^5$ [84] | $10^7$-$10^8$[85] | $10^7$[86] |
| $J_C(5T)/J_C(0)$ | 0.2 | 0.5 | 0.5 | 0.2-0.5 | 0.003-0.1 |

Just to mention not all but few similarities and differences between cuprates and iron-based superconductors as listed below.

**Differences**

I. Cuprates are Mott-insulator with delocalized electron while Iron pnictides are poor metallic compounds with itinerant electrons [87, 88].
II. Application of pressure on cuprates enhances Tc but not appearance of superconductivity; on the other hand in iron pnictides it results in superconductivity [89].
III. The cuprates have single band at the Fermi energy when compared with the iron pnictides which has multiple bands [90].

**Similarities**

I. Both compounds have layered structure. They consist of FePn- or FeCh-layers (iron-pnictogen or chalcogens). Which dominate the electronic states at the Fermi level and produce superconductivity [91].
II. Both have a dome shaped transition temperature. Superconductivity increases with doping until an optimum doping limit is reached and then decreases with an increase in doping concentration [92].

### 2.2.5 The $Ba_xFe_2As_2$ superconductor.

This part specifically highlights aspect and properties of $BaFe_2As_2$ material also known as Ba122 with a Tc of 38 K, [18]. The material has a tetragonal $ThCr_2Si_2$ structure which belongs to the family of 122 with a chemical composition $AFe_2As_2$ (A = Ba, Ca, Eu). It is a two dimensionally layered structure as shown in Figure 2.7 and is built up by layers of edge sharing FeAs tetrahedra simply with an alternating of Barium atoms and it is non superconducting at ambient pressure.

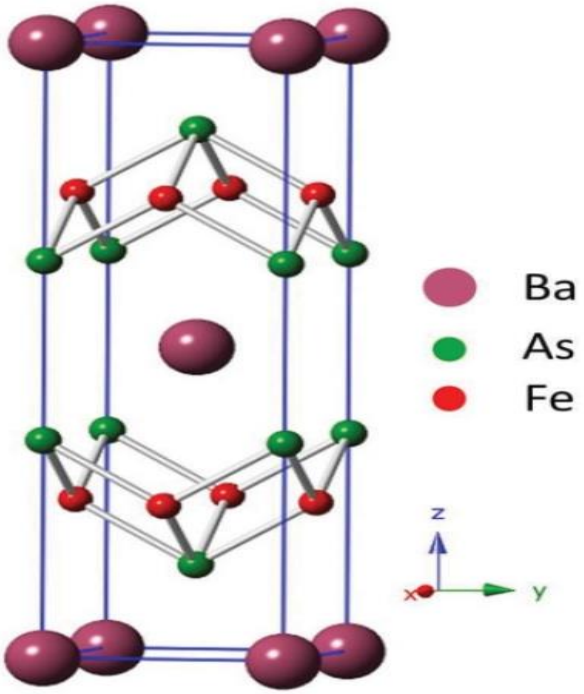


Figure 2.7. Crystal structure of layered BaK122 material [93].

Just like any other iron based superconductors, the parent compound is metallic with itinerant magnetic moment and superconductivity follows the BCS theory [94]. The non-superconducting behavior is the result of the spin density wave. The Ba122 compound has the highest current density amongst the other types (111 and 11) of about $3\times10^{5}$ $Acm^{-2}$ (5 K) [72, 73]. It has been found that Ba122 material has the second highest Tc of 38 K, having 111 types being the first with a highest Tc of 55 K.

The synthesis of this material has already been reported during the past years, however no physical properties where known except for the crystal structure and some indeterminate magnetic data [95]. Excluding the closely related geometry of the crystal structures, LaFeAsO and $BaFe_2As_2$ have identical electron counts of FeAs layers in both cases one electron is transferred to the FeAs sheets according to $(LaO)^{+}(FeAs)^{-}$ and $Ba_{0.5}^{2+}$ $(FeAs)^{-}$, respectively.

## 2.2.6 Pinning in $BaFe_2As_2$.

Fe-based superconductors are found to show a low anisotropy in doped $BaFe_2As_2$ also referred to Ba122. It was discovered that doping the latter with K, will results in maximum Tc of about 35 K and this will induce a very strong intrinsic pining strength with high critical

current density and $H_{c2}$ simultaneously [96], however other magnetic dopants like Co and Ni lead to a low Tc between 18-22 K and also they have low $J_c$ and $H_{c2}$ as compared to K doped 122, although the grain boundaries are not detrimental to the Jc, as it has been reported for Co-doped 122 epitaxial thin films [87].

The fundamental properties of the two layers Ba arsenide (122) have been extensively investigated due to the availability of good quality single crystals. The high Jc of about $10^{-5}$-$10^{-6}$ $A/Cm^2$ in seemingly defect free single crystals of doped BaFe2As2 (Ba122) is surprising and elicits questions on the origin of flux pinning centers in these materials [97,98]. So far little work has been done on the pnictides compounds however it has been found that pining in this material is much stronger than pining in cuprates superconductors [60].

## 2.2.7 Reference


1. Bednorz, J.G., and Muller K.A. Z: cond. Matt 64. 189 1986.
2. Chu, C.W., Hor, P.H., Gao, M.L., Huang, Z.J., and Wang, Y. Q.: Phys. Rev. Lett 58. 405 1987.
3. Maeda, H., Tanaka, Y., Fukutomi, M., and Asano, T.: Jpn. J. Appl. Phys, 27 L209 1988.
4. Sheng, Z., and Hermann, A. M.: Appl. Phys. Lett 52 1738 1988.
5. Putlin, S.N., Antipov, E.V., Chmaissem, O., and Marezio. Natt. 362 226 1993.
6. Takeshita, N., Yamamoto, A., Iyo, A., and Eisaki. Phys. Soc. JP 82 023711 2013.
7. Deutscher, G., and Muller, K.A. : Phys. Rev. Lett.. 59 1745 1987.
8. Itoh, K.I., Hashizume, A., Konmoto, H., Matsuo, M., Endo, T., and Mukaida, M.: Physiica C 357-360 477 2001.
9. Dulcic, A., Crepeau, R. H., and Freed, J.H.: Phys. Rev. B 42 2155 1990.
10. http://www.pha.jhu.edu/~vstanev1/#DIFERENT_PHASES
11. Eisaki H et al.: effects of chemical inhomogeneity in bismuth-based copper oxide superconductors. Phys. Rev B 69(6): 064512-1-064512-8.
12. Neven, B., Mun, K. Chan, Yuan Li, Guichuan Yu, Xudong Zhao, Martin Dressel, Ana Smontara, and martin Greven.: PNAS. Vol 110 NO 3, 12237 (2013).
13. https://bib.irb.hr/datoteka/632036.Barisic-PNAS-2013.pdf
14. Kamihara, Y., Walanabe, T., Hirano, M., and Hosono, H.: J. Am chem soc.130, 3296 (2008).
15. Chen, X.H., Wu, T., Wu, G., Liu, R.H., Chen, H., and Fang, D.F.: Nature (London) 435,761(2008).
16. Zhao, J., Huang, Q., Li, s., Lann, J.w., Chen, Y., Green, M.A., Chen, G.F., Li, G. , Li, Z., Luo, J.L., Wang, N.L., and Dai, P.: Nature mater 7, 953(2008).
17. Ren, Z., Tao, Q., Jiang, S., Feng, C., Wang, C., Dai, J., Cao, G., and Xu, Z.: Phys. Rev. Lett. 102, page 37002 (2009).
18. Rotter, M., Tegel, M., and Johrendt, D.: Phys. Rev. Lett. 101, 107006 (2008).
19. Wang, X.F., Wu, T., Wu, A., Liu, R.H., Chen, H., Xie, Y.L., and Chen, X.H.: New journal of physics, 11: 045003, 2009.
20. Yin, Z.P., lebegue, S., Han, M.J., Neal, B.P., Savrasov, S.Y., and Pickett W.E.: Phys. Rev. Lett.101 page 047001, 2008.

21. Gavaler, J.R.: superconductivity in Nb3Ge films above 22K. Appl. Phys. Lett., 23:480 1973.
22. Bednorz J.G., and Muller, K.A.: Possible high Tc superconductivity in Ba-La-Cu-O system. Z. Phys. B, 64(2):189, 1986.
23. Wu, M.K., Ashburn, J.R., Torng, C.J., Hor, P.H., Meng, R.L, Gao, L., Huang, Z.J., Wang, Y.Q., and Chu, C.W.: Superconductivity at 93K in a new mixed –phase Y-Ba-Cu-O compound system at ambient pressure. Phys.Rev .Lett. 58(9):908-910, march 1987.
24. Dai, P., Chakoumakos, B.C., Sun, G.F., Womg, K.W., Xin, Y., and Lu, D.F.: Synthesis and neutron powder diffraction study of the superconductor HgBa2Ca2Cu3 by T1 substitution. Physica C: superconductivity, 243:201, 1995.
25. Gao, L., Xue, Y.Y., Chen, F., Xiong, Q., Meng, R.L., Ramirez, C., Chu, W., Eggert, J.H., and Mao. H.K. Superconductivity up to 164K in HgBa2 (m=1, 2, and 3) under quasihydrostatic pressures. Phys.Rev, 50(6):4260-4263, 1994.
26. http://en.wikipedia.org/High-temperature-superconductivity
27. Abrisokov, A.A., and Gorkov, L.P.: Contribution to the theory of superconducting alloys with paramagnetic impurities. Sov. Phys. JETP, 12:1243, 1961.
28. Wang, C., Li, L., Chi, S., Zhu, Z., Ren, Z., Li, Y., Wang, Y., Lin, X., Luo, Y., Jiang, S., Xu, Z., Cao, G., and Xu Z.: Euro Phys. Lett. 83, 67006 (2008).
29. Chen, X. H., Wu, T., Wu, G., Liu, R. H. , Chen, H., and Fang D. F.: Nature 453, 761 (2008).
30. Chen, G. F., Li, Z., Wu, D., Li, G., Hu, W. Z., Dong, J., Zheng, P., Luo, J. L., and Wang N. L.: Phys. Rev. Lett 100, 247002 (2008).
31. Ren, Z.-A., Yang, J., Lu, W., Yi, W., Shen, X.-L., Li, Z.-C., Che, C.-C. , Dong, X.-L., Sun, L.-L., Zhou, F., and Zhao Z.-X.: Euro Phys. Lett. 82, 57002 (2008).
32. Rotter, M., Tegel, M., Shellenberg, I., Hermes, W., Pottgen, R., and Johrendt, D.: Phys. Rev. B 78, 020503 (2008).
33. Chen, G. F., Li, Z., Li, G., Hu, W. Z., Dong, J., Zhang, X. D., Zheng, P., Wang, N. L., and Luo J. L.: Chin. Phys. Lett 25, 3403 (2008)
34. Sasmal, K., Lv, B., Lorenz, B., Guloy, A., Chen, F., Xue, Y., Chu, C. W.: Phys. Rev. Lett 101, 107007 (2008)
35. Wu, G., Chen, H., Wu, T., Xie, Y. L., Yan, Y. J., Liu, R. H., Wang, X. F., Ying, J.J., and Chen X. H.: J. Phys.: Condens. Matter 20 ,422201 (2008).
36. Jeevan, H. S., Hossain, Z., Geibel, C., Gegenwart P.: Phys. Rev. B 78, 092406 (2008).

37. Sefat, A. S., Jin, R., McGuire, M. A., Sales, B. C., Singh, D. J., and Mandrus D.: Phys. Rev. Lett 101, 117004 (2008).
38. Wang, X.C., Liu, Q.Q., Lv, Y.X., Gao, W.B., Yang, L.X., Yu, R.C., Li, F.Y., Jin C.Q.: Solid State Communications 148, 538 (2008).
39. Hsu, F.-C., Luo, J.-Y., Yeh, K.-W., Chen, T.-K., Huang, T.-W., Wu, P. M., Lee, Y.-C., Huang, Y.-L., Chu, Y.-Y., Yan D.-C., and Wu, M.-K.: Proc Natl. Acad. Sci. USA 105, 14262 (2008).
40. Paglione, J., and Greene, R. L.: High temperature superconductivity in iron based materials. Nature physics, 6(9): 645-658, September 2010.
41. www.google.co.za/search?q=structure+of+iron+based+pnictides dates:02/09/2015
42. www.google.co.za/#q=phase+diagram++of+iron+based+pnictides dates: 02/09/2015
43. Johnston, D.C.: The puzzle of high temperature superconductivity in layered iron pnictides and chalogenides. Advances in Phys 83, 1589-1652 2011.
44. Stewart, G.R.: Superconductivity in iron compounds reviews of modern physics 83 1589-1652 2011.
45. Ksenofontov, V. et al.: Superconductivity and magnetism in $Rb_{0.8}Fe_{1.6}Se_2$ under pressure. Physical reviews B 85, 214519 2012.
46. Marsik, P. et al: coexistence and competition of magnetism and superconductivity on nanometre scale in under doped $BaFe_{1.89}Co_{0.11}As_2$. Physical review letters, 105, 057001. 2010.
47. Park, J.T. et al.: Electron phase separation in the slightly under doped iron pnictides superconductor $(Ba_{1-x}K_x)Fe_2As_2$. Physical review letters, 102. 117006 2010.
48. Li, Z. et al.: Microscopic Coexistence of antiferromagnetic order and superconductivity in Ba0.77K0.23Fe2As2. Physical review B 86 180501 2012.
49. Ma, L. et al.: Microscopic coexistence of superconductivity and antiferromagnetic in under doped Ba $(fe_{1-x}Ru)_2As_2$. Physical review letters, 109 197002. 2012.
50. Rotter, M., Pangerl, M., Tegel, M., and Johrendt, D.: Angevu chem. Int. Ed. Engl. 47 7949-52, 2008.
51. Chu, J.H., Analytis, J.G., Kucharczyk, C., and Fisher, I.R.: Phys. Rev. B 79 014506 2009.
52. Jiao, L., Zhang, J.L., Balakirev, F.F., Chen, G.F., Luo, J.L., Wang, N.L., and Yuan, H.Q.: J. Phys. And Chem. Solids 72 423 2011.
53. Weiss, J.D., Tarantini, C., Jiang, J., Kametani, F., Polyanskii, A.A., Larbalestier, D.C., and Hellstrom, E.E.: Nat.mat 11 682.

54. Fang, L. et al. Nat. Commun 4 1347 2013.
55. Si W, Han, J., Shi, X., Ehrlich, S.N., Jaroszynski, J., Goyal, A and Li, Q. : Nat. Commun. 4 1347 2013.
56. Ren, Z-A. et al. Chin. Phys. Lett 25 2215 (2008).
57. Wang, C. et al. EPL 8367006 2008.
58. Lida, K. et al. : Nat 3. 2139 2013.
59. Moll, P.J.W., Puzniak, R., Balakirev, F., Rogacki, K., Karpinski, J., Zhigadlo, N.D., and Batlogg, B. : Nat. Mat. **9** 628 2010.
60. Panarina, N.Y. et al. : J. Phys. Conf. Series. 200 012154. 2010.
61. Puri M. et al.:Supercond. Sci. Technol. **23,** 034003 (2010).
62. Ren C. et al. : Phys. Rev. Lett. **101** 257006; (2008).
63. Orlando, T.P. : et al. : Phys. Rev. B **36** 2394;(1987), Nguyen P.P., et al. : Phys. Rev B 48 1148(1993) and Moodera J.S. : et al.: Phys. Rev. B **37** 619 (1988).
64. Tajima Y., et al. : Phys. Rev. B **37**, 7956 (1988).
65. Zimmermann, P., et al.: Phys. Rev. B **52** 541, (1995).
66. Welp, U. et al. Phys. Rev. Lett. **62** 1908, (1988).
67. Putti, M. et al. Supercond. Sci. Technol. **21**, 043001, (2008).
68. Zehetmayer, M. et al. Phys. Rev. B **66**, 052505, (2002).
69. Kusmartsev, F.V.: Phys. Rev. Lett **68** 2268 1992.
70. Graser, S. et al. : Nature Phys. **6** 609, (2010).
71. Moll P.J.W. et al. : Nature Mat. **9**, 628, (2010).
72. Yang, H. et al. : Appl. Phys. Lett. **93**, 142506, (2008).
73. Yamamoto, A. et al. : Appl. Phys. Lett. **94**, 062511, (2009).
74. Taen, T. et al. : Phys. Rev. B **80**, 092502, (2009).
75. Lan, M.D. et al. : Phys. Rev. B **44**, 233, (1991).
76. Eisterer, M. : Supercond. Sci. Technol. **20**, R47, (2007).
77. Tanatar, M.A. et al. : Phys. Rev. B **79**, 094507 (2009).
78. Cabtree, G.W et al. : Phys. Rev. B **36**, 4021, (1987).
79. Santhanam et al. : Science News 131, 308, (1987).
80. Kidsum, M. et al. : Phys. Rev. Lett. **106**, 137001 (2011).
81. Lee, S. et al. : Nature Mat. **9**, 397, (2010).
82. Katase, T. et al. : Appl. Phys. Express **3**, 063101 (2010).
83. Tarantini, C. et al. : Appl. Phys. Lett. **96**, 142510 (2010).
84. Li, Q. et al.: Rep. Prog. Phys. **74**, 124510, (2011).

85. Dam, B.  et al. : Nature 399, 439, (1999).
86. Xi, X.X. : Supercond. Sci. Technol. **22**, 043001, (2009).
87. Katase, T., Ishimaru, Y., Tsukamoto, A., Hiramatsu, H., Kamiya, T., Tanabe, K., and Hosono, H. : Nat. Commun. DOI: 10.1038/ncomms 1419 2011.
88. Si, Q.: Nat. Phys. **5** 629.
89. Kreyssig, A. et al. Phys. Rev. B **78** 184517 2008.
90. Hyungju, O., Moon, J., Shin, D., Moon, C-Y., and Choi H.: Prog. Supercond. **13** 65 2011.
91. Lee, H., Kihou, K., Iyo, A., Kito, H., Shirage, P.M., and Eisaki, H.: solid state Commun. 152 644 2012.
92. Huang, Q., Zhao, J., Lynn, J.W., Chen, G.F., Luo, J.L., Wang, N. L., and Dai, P.: Phys. Rev. B 80 220503(R) 2009.
93. stacks.iop.org/JPhysCM/21/012208
94. Bardeen, J., Cooper, L.N., and Schrieffer, J.R.: Microscopic theory of superconductivity. Phys. Rev. 106 (1): 162-164 1957.
95. Wang, C., Gao, Z., Yao, C., Wang, L., Qi, Y., Wang, D., Zhang, X., and Ma, Y.: Supercond. Sci. Technol. 24 065002 (2011).
96. Wang, X.L., Ghorbani, S.R., Lee, S-I., Dou, S.X., Lin, C.T., Johansen, T.H., Muller, K.H., Cheng, Z.X., Peleckis, G., Shabazi, M.: Phys. Rev. B 82 024525 (2010).
97. Sun, D.L., Liu, Y., and Lin, C.T.: Phys. Rev. B. 80 144515 (2009).
98. Prozov, R., Tantar, M.A., Ni, N., Kreyssig, A., Nandi, S., Budko S.L., Goldman, A.I and Canfield, P.C.: Phys.Rev. B.80 174517 (2009).

# CHAPTER 3

## Literature survey on Non-Resonant Microwave Absorption in high $T_c$ superconductors.

Non-resonant microwave absorption in High Tc superconductors was first observed and published by Bhat et al [1] just soon after the discovery of high temperature superconductors by Bednorz and Muller. After that a number of reports then followed [2, 3, 4], and now technique is established to be very useful in the study of high temperature superconductors. We shall attempt to give a brief highlight of some of the important papers.

Portis et al [5] , has shown that the absoprtion in ceramic samples has a minimum at zero field and then increases smoothly with increase in applied magnetic field. This is attributed to fluxon motion driven by microwave currents. Line spectra are observed in single crystals instead of smooth absoprtion as a function of applied field [6, 7]. This kind of line spectra are not peculiarity of the high Tc superconductors but it has been found in the convectional superconductors such as Nb [8]. Their origin is thought to be microwave current induced nucleation and annihilation of fluxons within sections of josephson junction in a superconducting loop intersecting an applied magnetic field [6]

Microwave absorption lines in $YBa_2Cu_3O_7$ single crystals for H//ab at 2.6 K were observed by Dulcic et al [9]. The following brief explanation was taken from ref [10], the flux is quantized in the superconducting loop, there are phase jumps as the applied field increases, these phase jumps occurs when the field enclosed becomes an intergral multiple of the unit quantum of flux. These flux jumps occur in a very short time and therefore produce large voltage pulse given by

$$v(t) = -(h/2e)\frac{d\theta}{dt} \qquad (1)$$

When this occurs the critical current of the superconductor is exceeded and normal current flows which can absorb microwave energy. Thus the microwave absorption spectrum of this loop as a function of increasing dc magnetic field will be series of equally spaced sharpabsorption which are separated from each other by $\Phi_0 / A$ , in this case A is the area of the loop. The signal is thought to be an envelope of these superposed line absorption in the

case of pellets because of a distribution in the weaklink and different possible loop orienations with respect to the dc magnetic field.

### 3.1.1 Dulcic model

Dulcic et al [11] proposed electromagnetic power loss in a superconductor to occur in the inter-granular Josephson junction. It is well known that at lower magnetic field the weak links between the superconducting grains provide superconducting paths for the Meissner shielding across the whole sample [12]. Increasing magnetic field reduces the critical current of the junction by the reduction factor

$$\text{F (H)} = \left[\sin(\pi H / H_0) / (\pi H / H_0)\right] \qquad (2)$$

The critical current is dependent on the magnetic field and temperature, it can be expressed as: $I_C(H,T) = I_C(0,T)F(H)$ (3)

$H$ is the magnetic field, $T$ is the temperature [13].If a small modulation field is present, $F(H)$ becomes $F(H + H_M \cos w_M t) = F(H) + F'(H)H_M \cos w_M t$ (4)

The boundary current/shielding current if it is weakly modulated, it can be expressed as $I_b = I_C + I_m \cos w_M t$ (5)

$I_b$ is the net boundary current, $I_M$ is the modulation current due to small modulation field and $I_0$ is the boundary current in the absence of modulation field and only a DC field is present, the expression for microwave loss in the limit where $I_{M\square} I_0$ becomes [14]

$$S_m = \frac{\sqrt{(0.5 I^2{}_{mw} R)}}{((1/R)(\hbar/2e)\omega_{mw})^2} - \frac{I_C}{(1+\eta)^{\frac{3}{2}}}\left[\frac{-dl}{dH} H_{M+} I_M \sin\Phi_0\right]\cos w_M t \qquad (6)$$

Where the first term is the sweep independent term and it grows linearly due to the fact that the DC magnetic fields reduces the junction currents by diffraction reduction, the second term is derived assuming that the small modulation fields are only giving rise to a small oscillation across the junction[15].

In order to see the derivative-looking microwave absorption signals, the modulation magnetic fields should be high enough to suppress the boundary current effect (shielding effect) and

the NRMA signals are due to fluxons driven by RF/ microwave currents. This limit $I_M \geq I_0$, as well can be approached by increasing the temperature instead of increasing the modulation field amplitude, therefore at a given modulation field, $I_M$ is constant and $I_0$ is reduced by increasing the temperature to reach the limit $I_M \geq I_0$ .

### 3.1.2 The Portis model

According to the model of the microwave absorption originating in the diffraction effects, the width of the absorption decreases with an increase in frequency. The model used by Dulcic et al., [2], where the saturated field depends upon the weak link dimensions cannot justify the results but charging the frequency arise because of the diffraction effects. But Portis et al., [5] model discussed below shows that the large frequency dependence of the line shape. Near the absence of hysteresis both in the microwave and the radio frequencies suggest that we are almost completely in the flux flow regime. In such a situation we are justified in taking $B \square H$ then, the surface resistance $R$ Arising from the damped motion of the fluxons is given by

$$R = X_0\left[(-1+\frac{\sqrt{1+4f^2B^2/B_0}}{2}\right]^{\frac{1}{2}} \qquad \text{And} \qquad X = X_0\left[1+\frac{\sqrt{4f^2B^2/B_0{}^2}}{2}\right]^{\frac{1}{2}} \qquad \text{where}$$

$X_0 = \left[4\pi\omega\mu\lambda_L / c^2\right]\mu^{\frac{1}{2}}$ is the impedance at zero magnetic fields, B the flux density, and $f$ the fraction of free fluxons. The permeability $\mu$ , defined by the relation $B = \mu H$ is $\square 1, \omega$ is the frequency of electromagnetic radiation.

### 3.1.3 Non-Resonant Microwave absorption features.

Below we attempt to summarize some of the important features of Non-Resonant Microwave absorption.

### (a) Modulation effects.

Several authors have reported that at a very low modulation field of about 0.05 the phase of the absorption derivative reverses as the swept dc field is reversed [1, 2, 5, 7]. Rakvin et al has noted the sign change of the force constant. The reverse critical state was attributed by Blazey et al [17]. Dulcic et al and Srinivasu et al also noted the boundary current effect respectively [14, 15] .This anomalous feature has been noted in different forms of sample [18, 19]. In powder sample of YBCO superconductor the signal evolves with rf power whereby at lower rf power, the rf absorption has a minimum at zero dc field, $H_{dc}$, and increases monotonically with increasing $H_{dc}$. At higher rf power level the phase is reversed.

### (b) Variety of the line shapes.

Dulcic et al has observed different kinds of line shapes in YBCO single crystals [16]. Near $T_c$ the derivative signals are very broad and flat, and far below $T_c$ are very narrow. Blazey et al [8, 17] has noted that the lines can be fitted by the expression $H\cos\theta = \pm(p+1/2)\Delta H$, they further explained that the lines were connected with the motion of fluxons into the regular arrays of twin planes. Owen has explained the spectral lines to be emerging from the phase jumps in a superconducting loop [10]. The phase jumps are experienced as the applied field is increases; this is due to the flux which is quantized in a superconducting loop. The phase jumps occurs when the field enclosed becomes an integral multiple of the unit quantum of flux.

### (c) Josephson junction noise and particle size.

Josephson junction noise was observed in the magnetically modulated microwave absorption (MAMMA) spectrum and it strongly lean on the particle size, the noise decreases as the particle size decreases [20].

## (d) Peak in absorption derivative Vs temperature.

Blazey and Hohler reported a sharp peak near Tc in YBCO thin films as the absorption derivative is plotted against the temperature [21]. As the modulation field is increased from 100 m Oe to 50 Oe the peak position is noted to shift towards lower temperature. Hence this was noted to the $k''$ (imaginary part of the ac susceptibility) peak. According to Blazey and Hohler such a peak is absent in ceramic pellets.

## (e) Surface barrier effect.

Srinivasu et al has reported the observation of the effects of surface barriers in thin single crystalline films of $YBa_2Cu_3O_{7-\delta}$ using the technique of NRMA, Surface barriers arises as a result of vortex with its mirror image and shielding currents on the surface. It was noted that there was a vertical hysteresis (unlike unilateral hysteresis due to bulk pinning) which increases unusually with an increase in temperature of the sample, this was noted to be from the difference in magnetization in forward and reverse field sweeps which agrees with one of surface barrier characteristics [22] .

## (f) Large ac loss in Superconducting.

A unique behavior on radio frequency measurement of BSCCO material was observed by Chockalingam et al [23]. A larger ac loss in the superconducting state was noted as compared to the normal state. They also detected two distinct peaks namely; peak A and peak B as indicated their work. Furthermore they observe a decrease in amplitude of peak A with increasing magnetic field. When the orientation of the sample is changed from o0 to 900 the amplitude increases. The unusual ac loss in the superconducting state was explained in terms of repeated coupling and decoupling of Josephson junction. Peak A is interpreted in terms of critical current density corresponding to the coupling energy, and Peak B arises as a result of Lorentz-force-driven motion of vortices [23, 24].

## (g) Paramagnetic Meissner effect.

Paramagnetic Meissner effect also known as Wohlleben effect is an uncommon paramagnetic response of a given superconducting samples of high temperature superconductors to an application of weak magnetic field [25, 26]. Anomalous microwave absorption that has a local maximum absorption at zero applied magnetic fields instead of a minimum absorption was shown in samples with Paramagnetic Meissner effect.

Some studies indicate that paramagnetic Meissner effect comes as a result of presence of $\pi$ junctions [27]. The effect is extrinsic and is associated with certain mesoscopic defect structures that favor formation of spontaneous orbital currents in the ground state this was pointed by Braunisch W et al [28]. Knauf et al highlighted that the critical current density of the $\pi$ junctions involved with spontaneous currents must be of order $10^5$-$10^6$A/cm$^2$ and the different sizes of grains of Bi2212 shows this effect. As a result they concluded that this large current is from the $\pi$ junction in intragrain rather than intergrain. And furthermore they observed that this effect is anisotropic in nature.

## (h) Oxygen deficiency.

Puri et al highlighted modulated microwave absorption studies on YBCO superconductors which shows a periodic oscillation with two different frequencies which they designated as signal type A and type B in their work [29]. They interpreted that there is at least two different kinds of microwave sensitive Josephson junctions that the oscillation might be coming from. Furthermore they observed different dependences on microwave power, temperature and field modulation in both signals. They came up with an idea that in YBCO single crystals oxygen deficiency act like Josephson junctions which bring the field microwave absorption noted.

## (i) Magnetic shielding.

Srinivasu et al has explore in detail the effect of magnetic shielding on pure YBCO thin film and silver doped YBCO thin film superconductors at both small and high field modulation [15]. They found better shielding in Ag doped YBCO when compared to undoped YBCO thin films, they noted that this difference is due to the improved microstructure in Ag-doped YBCO resulting from good grain alignment and grain enlargement.

## (j) The second and third peak.

2$^{nd}$ and 3$^{rd}$ peak which evolves with microwave power has been noted in Bi2212 single crystals, these two peaks have been attributed to microwave losses resulting from decoherence and destroying of the otherwise microwave power induced phase locking of junctions [30].

Rastogi et al [31] and many other authors [30- 34], have observed 2$^{nd}$ peak. However according to Rastogi et al the 2$^{nd}$ peak arises from intrinsic Josephson coupling between

$Cu_2O$ layers while another author known as Masiakowski et al [32] has suggested that the 2nd peak originate from second phase in the sample. However Srinivasu et al [33] has showed that not only does this 2nd peak depend on mutual orientations of the crystals ab plane, the DC field and magnetic field but also it depends on microwave power.

## (k) Magnetic hysteresis.

Several authors have observed high temperature superconductors which show anomalous hysteresis where the forward curve lies above the reverse curve when magnetic field is swept forward and reverse [35 - 38]. Tripathy et al [36] has noted that in BSCCO magnetic hysteresis originate from absorption response in different types of Weaklinks forming Josephson junctions. The observed signal was calculated systematically by the combination of Portis and Dulcic model.

The anomaly has been interpreted that it occurs as a result of fluctuation coming from layered structures and high anisotropy when the magnetization measurements are done on the same superconductor material [37]. The generation and detection of energy stabilized Josephson junction fluxons maybe the cause of the anomaly, this has been argued by Padam et al [38].

The hysteresis is magnetic field sweep dependent, this was noted by Mahel et al [39]. They further disclose that in Non-resonant microwave absorption the hysteresis is due to the formation of critical states in the Weaklinks network and the interaction between the inter and intra-grain vortices.

In the micron sized powders of $YBa_2Cu_3O_7$ Gould et al [40] have observed strong magnetic field hysteresis in low field microwave absorption. It was found to be a strong function of temperature and microwave frequency. This hysteresis (measured at 1.3 K and at 35 GHz microwave frequency and as well as in zero field cooled samples) is of conventional type, given the minimum in the microwave absorption in the forward scan ( field swept from -80 Oe to +80 Oe) occurred at +50 Oe. The same applies to the reverse sweep, where the minimum occurred at -50 Oe. The hysteresis vanished when the temperature was increased to about 16 K and above that is both the reverse and forward field sweep minima occurred at the zero of the applied field. By keeping the temperature constant at about 1.4 K and the microwave frequency decreased to 10 GHz, the strong hysteresis that appears at 35 GHz and at a temperature of 1.3 K disappeared, and both the forward and reverse sweep minima occurred at zero of the applied magnetic field. Lastly they also note that the field cooling

shifts the absorption minima in the direction of the cooling field. They attribute these effects to the spin glass nature of the sample.

## (l) Observation of a structure and line shape evolution in iron Pnictides

R.B Onyancha et al [41] have reported on the non-resonant microwave absorption in $SmFeAsO_{0.88}F_{0.12}$ polycrystalline sample measured at 9.45 GHz below $T_c$ (6.06- 42 K). They observed a line shape structure with remarkably two peaks, namely; a broad peak 1 and a narrow peak 2. They found that the structure and the line shape were evolving as a function of temperature and field modulation, furthermore they found that there is no crossover of NRMA signals from normal to anomalous type as a function of temperature which is totally different compared to the NRMA in cuprates.

## (m) Critical current density

Srinivasu et al [42] discovered the new contact-less technique for the measurement of the critical current density $J_c$ using Non resonant microwave absorption based method for the determination of $J_c$ in the high Tc superconductors. The method was shown to give values of Jc comparable to those determined by the transport current method. Furthermore Srinivasu et al [43] have observed the highest values of $J_c$ ($\sim 10^5 A/cm^2$) in a large area of approximately ($\sim 1.2 cm^2$) films, using the non-resonant microwave absorption technique in high pressure oxygen sputtered thin films of YBCO superconductor.

### 3.1.4 Refernces


1. Bhat, S.V., Ganguly, P., and Rao, C.N.R., and Pramana. J.Phys. 28 L425 (1987)
2. Bhat, S.V., Ganguly, P., Ramakrishnan, T.V., and Rao, C.N.R.: J. Phys. C 20 L539 (1987).
3. Blazey, K.W., Muller, K.A., Bednorz, J.G., Berlinger, W., Amoretti, G., Buluggiu, E., Vera, A., and Matacotta, F.C.: Phys. Rev. B36 7241 (1987).
4. Orlandi, P., and Rigamonti, A.: Physica C 178 197 (1991).
5. Portis, A.M., Blazey, K.W., Muller, K.A., and Bednorz, J.G.: Euro. Phys. Lett . **5** 467 (1988).
6. Blazey, K.W., Portis, A.M., Muller, K.A., and Holtzberg, F.H.: Europhys. Lett. **6** 457 1988.
7. Dulcic, A., Crepeau, R.H., and Freed, J.H.: Phys. Rev. B **39** 4249 (1989).
8. Blazey, K.W., Portis, A.M., Muller, K.A., and Holtzberg, F.H.: Europhys. Lett.**6** 457 (1988), Blazey, K.W., Portis, A.M., and Holtzberg, F.H.:Physica C 157 (1989).
9. Dulcic, A., Crepeau, R.H. , Freed, J.H., Schneemeyer, L.F., Waszczak, J.V.: Phys. Rev . **42** 2155 (1990).
10. Frank, J., Owens: Physica C **171** 25 (1990).
11. M. Puri et al., Supercond. Sci. Technol. **23**, 034003 (2010).
12. Hsu, F.-C., Luo, J.-Y.,. Yeh, K.-W., Chen, T.-K., Huang, T.-W., Wu, P. M., Lee, Y.-C., Huang, Y.-L., Chu, Y.-Y., Yan, D.-C., and Wu, M.-K.: Proc Natl. Acad. Sci. USA **105**, 14262 (2008).
13. Gavaler, J.R.: Superconductivity in Nb3Ge films above 22 K. Appl. Phys. Lett. **23**. 480, 1973.
14. Dulcic, A., Rakvin, B., and Pozek, M.: Europhys. Lett. **10**, 593 (1989).
15. Srinivasu, V.V., Pinto, R., Sastry M.D.: Applied superconductivity volume 4 number 4 pp. 195-201, (1996).
16. Dulcic, A. Crepaeu, R.H., and Freed, J.H.: Phys. Rev. B **38** 5002 (1989).
17. Blazey, K.W., Portis, A.M., and Bednorz, J.G.: Solid state Commun. **65** 308 (1988).
18. Bhat, S.V., Srinivau, V.V, and Kumar N..: Phys. Rev **44** 10121 1991.
19. Srinivasu, V.V., Bhat, S.V., and Kumar, N.: solid state Commun. 89 375 1994.

20. Bohandy, J., Kim, B.F., Andrian, F.J., and Moorjani, K.: Phys. Rev. B 39 2733 1989.
21. Blazey, K.W., and Hohler, A.: Solid State Commun. **72** 1199 (1989).
22. Rastogi, A., Srinivasu, V.V., Hedge, M.S., and Bhat, S.V.,: Physica C **234** 229. 1994.
23. Chockalingam, S.V., Saragi, S., Bhat, S.V., Oka, K., and Nishihara, Y.: J. Phys. Condens. Matter **21** 045704. 2009.
24. Saragi, S., Chockalingam, S.P., and Bhat, S.V.: J. Phys. **98** 073906 2005.
25. Knauf, N et al: Europhys. Lett. **55** 541. 1996.
26. Knauff, N et al : Physica C **399** 125 . 1998.
27. Bhat, S.V., Rastagi, A., Kumar, N., Nagarajan, R., and Rao, C.N.R.: Physica C **219** 87. 1994.
28. Kusmartsev, F.V.: Phys. Rev. Lett **69** 2268. 1992.
29. Puri, M., Durny, R., and Kevan L.: Physica C **190** 210 1992.
30. Srinivasu , V.V.: J. Supercond.Nov.Magn. **23** 305 2010.
31. Rastogi, A., Sudershan, Y.S., Bhat, S.V., Grover, A.K., Yamaguchi, Y., Oka, K., and Nishihara, Y.: Phys. Rev. B **53** 9366 1996.
32. Masiakowski, J.T., Micky, P., and Larry, K.: J. Phys.Chem. **95** 1393. 1991.
33. Srinivasu, V.V. et al : J.Supercond. Nov. Magn. **14** 41 2001
34. Wu, C.J., and Chen, Y. L.: Prog. Electromagn. Res. **111** 433 2011.
35. Ji, L., Rzchowski, M.S., and Anand, N., and Tinkham, M.: Phys. Rev. B **47** 470 1993.
36. Tripathy, M.R., Srivastava G.P.: Ieee. Trans.Magn. **35** 4079 1999.
37. Pradhan, A.K, Roy, S.B., Chaddah, P., Chen, C., and Wanklyn, B.M.: Phys. Rev. B. **52** 6215 1995.
38. Padam, G.K., Arora, N.K., and Ekbote, S.N.: Mat. Chem and Phys. **123** 752 2010.
39. Mahel, A., Hlubina, R., and Benacka, S.: Physica C **169** 429 1990.
40. Gould, A., Bhagat, S.M., Manheimer, M.A., and Tyagi, S. :J. Appl. Phys. **67** 5020 1990.
41. Onyancha, R.B., Shimoyama, J., Singh, S.J., Ogino, H., Srinivasu, V.V.: J. Supercond. Nov. Magn. **28** 2927-2934 2015.
42. Srinivasu, V.V., Thomas, B., Vasanthacharya, N.Y., Hedge, M.S., and Bhat, S.V.: Solid State Commun. Vol 79. No 9 713-716 1991.

43. Srinivasu, V.V., Bhat, S. V., Muralidhar, G.K., Mohan, G., and Mohan, S.:J. Phys. Vol 40. No 2 119-122 1993.

# Chapter 4

## Sample characterization

High quality single cryatals are essential for advanced scietinfic research, many scientist tried to grow single crystals of iron based supercondctors, however it is found that to grow sizable single crystals of the Fe1111 type (LnFeAsO) and AFeAsF is quite difficult.

Fortunately big single crystals of Fe-122 type (AFe2As2) can be grown using additional metal as flux or by self flux method. Hence with this success, more accurate meausrements have become possible on this iron-based superconducting system. The upper critical field and its anistropy are fundamental parameters of each superconductor, and they are crucial for both understanding the superconducting mechanism and the potential applications.

In this chapter, we give details about the growth, characterization of the superconducting properties of BaK122 single crystals. We have make use of the following equipments which are available in ou lab: XRD, PPMS and EPR.

## 4.1 Single crystal growth.

The single crystals of BaK122 were synthesized through a self-flux method, the FeAs precursrsor was synthesized by the reaction of Fe powder (Alfa Aesar, 99.99% in purity) and As chips(99.9%) with a ratio of 1:1, were heated to a temperature of $900^0$C for 10 hours in a sealed silica tube. The starting materials of Ba fillings (1.758g), Fe Powder (2.38g), As (3.358g) and soft bulk of the proper amount of potassium pieces (0.5g) was added to cover the powder. The whole procedure was carried out in a glove box with a protective Argon atmosphere in which the concentration of both $O_2$ and $H_2O$ were less than 1 ppm, the mixture was then ball milled for 9 hours, until it was in a homogeneous state, Then the mixture was placed inside the crucible and sealed inside the iron metal tube, the reason we used the iron metal tube is because the silica tube would break due to the gas pressure of potassium at a temperature around 1000 $^0$C. The sealed iron metal tube was placed in a tube furnace and heated starting from a room temperature of about $8^0$C up to $710^0$C for 5 hours, holding for 200 minutes, and then continue heating for another 2.5 hours up to $1180^0$C, holding for 5 hours. It was cooled down to a temperature of $1050^0$C for 39 hours, then for 2 hours to $800^0$C, then lastly it was cooled for another 2 hours to $20^0$C , finally the tube furnace was powered off, after that the tube was cooled down to a room temperature, then it was broken

down. The crystals were obtained by cleaving the As-grown bulks, and then they were selected and shaped under a microscope.

## 4.2 The Tube Furnace

Fig.4.1 Picture of the tube furnace [1].

A tube furnace is an electric heating device used to conduct syntheses and purifications of inorganic_compounds and occasionally in organic_synthesis. One possible design consists of a cylindrical cavity surrounded by heating coils that are embedded in a thermally insulating matrix. Temperature can be controlled via feedback from a thermocouple. More elaborate tube furnaces have two (or more) heating zones useful for transport_experiments. Some digital temperature controllers provide an RS232 interface, and permit the operator to program segments for uses like ramping, soaking, sintering, and more [2] . Advanced materials in the heating elements, such as molybdenum disilicide offered in certain models can now produce working temperatures up to 1800 °C. This facilitates more sophisticated applications. [3] Common material for the reaction tubes includes alumina, Pyrex, and fused quartz. The tube furnace was invented in the first decade of the 20th century and was originally used to manufacture ceramic filaments for Nernst_lamps and glowers [4].

An example of a material prepared using a tube furnace is the superconductor BaK122. A mixture of finely powdered Fe, Ba, and K and As, in the appropriate molar ratio, contained in a platinum or alumina "boat," is heated in a tube furnace at several hundred degrees under flowing oxygen. Tube furnaces can also be used for thermolysis reactions, involving either organic or inorganic reactants. One such example is the preparation of ketenes which may employ a tube furnace in the 'ketene lamp'. Flash_vacuum_pyrolysis often utilizes a fused quartz tube, usually packed with quartz or ceramic beads, which is heated at high temperatures.

## 4.3 X-Ray Diffraction.

Fig.4.2 Image of XRD [5]

Note the following brief explanation is taken from Diffraction Methods section of ASM Handbook, Volume 10 Materials Characterization [5].

X-ray diffraction techniques are some of the most useful in the characterization of crystalline materials, such as metals, inter metallic, ceramics, minerals, polymers, plastics, or other inorganic or organic compounds. X-ray diffraction techniques can be used to identify the phases present in samples from raw starting materials to finished product and to provide information on the physical state of the sample, such as grain size, texture, and crystal

perfection. Most x-ray diffraction techniques are rapid and non-destructive; some instruments are portable and can be transported to the sample. The sample may be as small as an airborne dust particle or as large as an airplane wing. In general, x-ray analysis is restricted to crystalline materials, although some information may be obtained on amorphous solids and liquids. XRD samples are acceptable in many forms, depending on the availability of the material and the type of analysis to be performed. Single crystals from a few microns to a few inches in diameter or loose or consolidated aggregate of many small crystals can be used. Although the overall size of the sample may be large, the actual area of the sample examined in a given experiment rarely exceeds 1 $cm^2$. The type of information obtained from x-ray diffraction studies ranges from sample composition to details of the crystal structure or the state of orientation of the crystallites. Phase identification can be conducted on virtually all single crystal or powder samples. Also useful are measurements of the physical state of a sample that detect differences from the ideal crystal (presence of defects, strain, etc.).

X-ray powder diffraction techniques are used to characterize samples in the form of loose powders or aggregates of finely divided material. These techniques cover various investigations, including qualitative and quantitative phase identification and analysis, determination of crystallinity, micro identification, lattice-parameter determinations, high-temperature studies, thin film characterization, and, in some cases, crystal structure analysis. The powder method is perhaps best known for its use as a phase characterization tool partly because it can routinely differentiate between phases having the same chemical composition but different crystal structures (polymorphs). Although chemical analysis can indicate that the empirical formula for a given sample is FeTiO3, it cannot determine whether the sample is a mixture of two phases (FeO and one of the three polymorphic forms of TiO2) or whether the sample is the single-phase mineral FeTiO3 or ilmenite. The ability of x-ray powder diffraction to perform such identifications more simply, conveniently, and routinely than any other analytical method explains its importance in many industrial applications as well as its wide availability and prevalence.

In x-ray powder diffraction analysis, samples usually exist as finely divided powder (usually less than 44 μm in size) or can be reduced to powder form. The particles in a sample comprise one or more independently diffracting regions that coherently diffract the x-ray beam. These small crystalline regions are termed crystallites. Consolidated samples, such as ceramic bodies or as received metal samples, will likely have crystallites small enough to be useful for powder diffraction analysis. The size limitation is important in x-ray powder

diffraction because most applications of powder diffraction rely on x-ray signals from a statistical sample of crystallites. Bragg's Law (Equation 1) states that the angular position, θ, of the diffracted x-ray beam depends on the spacing, d, between planes of atoms in a crystalline phase and on the wavelength, λ, of the x-ray, $n\lambda = 2d \sin\theta$

## 4.4 Physical Property Measurement System PPMS


Fig. 4.3 Picture of Physical Property Measurement System (PPMS) [6].

The following explanation is taken from Thermal Transport Option User's Manual Part Number 1684-100B [7].

The Quantum Design Thermal Transport option (TTO) for the Physical Property Measurement System (PPMS) enables measurements of thermal properties, including thermal conductivity κ and See beck coefficient (also called the thermos power) α, for sample materials over the entire temperature and magnetic field range of the PPMS. The TTO system measures thermal conductivity, or the ability of a material to conduct heat, by monitoring the temperature drop along the sample as a known amount of heat passes through the sample. TTO measures the thermoelectric See beck effect as an electrical voltage drop that

accompanies a temperature drop across certain materials. The TTO system can perform these two measurements simultaneously by monitoring both the temperature and voltage drop across a sample as a heat pulse is applied to one end. The system can also measure electrical resistivity ρ by using the standard four-probe resistivity provided by the PPMS AC Transport Measurement System (ACT) option (Model P600). All three measurement types are essential in order to assess the so-called "thermoelectric figure of merit," $ZT = \alpha^2 T/\kappa\rho$, which is the quantity of main interest if you are investigating thermoelectric materials.

The TTO system measures electrical resistivity ρ by using a precision DSP current source and phase sensitive voltage detection. The specifications for this AC resistivity measurement are essentially identical to those for the AC Transport Measurement System (ACT) option, because the same high performance hardware is used by both TTO and ACT.

## 4.5 Non- Resonant Microwave Absorption (NRMA) Technique.

The non-resonant microwave absorption technique is highly sensitive, contactless and non destructive way of characterising superconductors which was discovered by Bhat et al[8] and also been reported by many other authors [9-12]. Ever since it was discovered it has been widely used in characterizing high $T_C$ superconductors, effect of magnetic shielding [13], surface resistance [14], anisotropy [15], critical current densities [16], as well as studying the electromagnetic response of cuprates. Although other techniques such as AC susceptibility and DC susceptibility [17-19] are very good in studying the shielding effect in superconducting samples, however in this experiment the NRMA technique will be used because it gives the shielding effect information in the presence of microwave field [13]. The intensity and the shape of the NRMA signal depend upon various parameters such as temperature, dc mganetic filed, microwave power and also on the nature of a sample. This technique has been vey effective in distinguishing between the dissipation originating from intra and inter granular regions in superconducting samples [20].

The NRMA technique registers the field derivative of the microwave loss in a superconducting sample as a function of applied magnetic fields. The behavior of NRMA has been observed in many superconducting [21] and non superconducting [9]materials, but due to granularity, two dimensionality and layered structure in high temperature superconductor (HTSC), the fluxon structure, density and mobility becomes very different from what used to be in the conventional ones. The NRMA signal is very sensitive to variation of magnetic field

and temperature, hysteresis loop which is similar in appearance to the standard DC magnetic hysteresis of HTS materials [22]. Various models were proposed to explain the origin of NRMA signal, some of them were based on (i) induced currents through the weak links [23] and (ii) damped josephson motion of fluxon within josephson junction [24]. The signal was found to have the following characteristics (1) the signal occurs below the transition temperature $T_c$ that is in the superconducting state [8], (2) it is very sensitive to temperature variation, magnetic field modulation amplitude and microwave power [25], (3) it has different characteristics' depending on the nature of the sample whether a single crystal, polycrystalline or thin film [20, 26].

In our work we have used the Non-Resonant Microwave Absorption Technique which encompasses the use of the Electron Paramagnetic Resonances (study the properties of BaK122 single crystals) to record the Non- Resonant response with electromagnetic radiation as a function of temperature and magnetic field. Typically in commercials spectrometer works by varying the magnetic field and holding the frequency constant. EPR spectrometers working at frequencies ranging from several hundred MHz to several hundred GHz are in use. 1-2 GHz (L-band) and 2-4 GHz (S-band), 8-10 GHZ (X-Band), 3.5 GHz (Q-band) and 9.5 GHz (W-band). The most commonly used EPR spectrometer is in the range of 9-10 GHz(X-band).

Fig.4.5 Electron Paramagnetic Resonance Spectrometer: image taken from our Unisa lab.

In addition to what has been discussed above, the experiment entails use of low dc field of 0-500 G which is generated from electromagnets. The residual magnetic field in EPR is usually nullified by the use of Helmholtz coils which generates a negative field of about 50 gauss opposite to fields from electromagnets hence attaining zero field system. In our ESR spectrometer, the power supply can sweep the magnetic field from positive to negative side crossing the zero field. The dc field generated by the electromagnet is then field-modulated by using modulation coils.

Audio frequency (57Hz to a few kilo Hertz) signal are taken from an in-built oscillator in the lock-in-amplifier and then fed to a power amplifier. The output of the power amplifier is then fed to the modulation coils. Modulation field is collinear with the dc magnetic field. Klystron provides microwave for spin excitation and signal detection in the EPR spectrometer and a cavity is where a sample will be placed. The dc is ramped from -100 gauss to 100 gauss through zero fields. Now any loss in the sample will show up as loss in the cavity. This causes a change in voltage/current as function of dc field sweep and can be amplified then fed to the phase sensitive detector (lock-in- amplifier).

Lock in amplifier is then fed to an x-y recorder. The input of the lock-in-amplifier can be fed in parallel form to an oscilloscope or computer to give a signal. Low temperature measurements were done using an Oxford Cryostat with liquid He flow and controlling flow and heater.

## 4.6 Reference


1. Image taken from the Chinese Academy of Sciences Laboratory. Dates 16-01-2015
2. Corbett, J. D.: "Synthesis of Solid-State Materials" in Solid State Chemistry: Techniques, A. K. Chee than and P. Day, Eds. Clarendon, Oxford,. ISBN 0-19-855165-7. 1987
3. Harker, J. A. (December 1905). "On a New Type of Electric Furnace, with a Redetermination of the Melting-Point of Platinum". *Proceedings of the Royal Society A* **76** (507): 235–249. Bibcode:1905RSPSA..76...235 H. doi:10.1098/rspa.1905.0023
4. Revelli, J. F., "Tantalum Disulfide ($TaS_2$) and Its Intercalation Compounds" Inorganic Syntheses, volume 30, pp. 155. Doi:10.1002/9780470132616.ch32. 1995
5. Diffraction methods section of ASM Handbook, Volume 10 materials characterization.
6. Image taken from Unisa Lab: date 10/08/2015
7. Thermal Transport Option User's Manual Part Number 1684-100B
8. Bhat, S.V., Ganguly, P., and Rao, C.N.R., and Pramana. J.Phys. 28 L425 (1987).
9. Dunny, R., Hautala,J., Ducharme, S., Lee, B., Symko, O.G., Taylor, P.C., Zhen, D.J., and Xu, J.A.: Phys. Rev. B. 36 2361 1987.
10. Khachaturyan, K. Weber, E.R., Tejedor, P., Stacy, A.M., and Portis, A.M.: Phys. Rev. B. 36 8309 1987.
11. Rettori, C., Davidov, D., Belaish, I., and Felner, I.: Phys. Rev. B. 36 4028 1987.
12. Sastry, M.D., Dalvo, A.G.I., Babu, Y., Kadam, R.M., Yajhmi, J.V., and Lyer R.M.: Nat 330 49-51 1987.
13. Srinivasu, V.V., Pinto, R., Sastry M.D.: Applied superconductivity volume 4 number 4 pp. 195-201, (1996).
14. Srinivasu V.V., Raychaudhuri, P., Souza, C.PD., Pinto, R., and Vijayaraghavan R.: Solid state Commun. Vol 102 No 5 409-412 1997.
15. Srinivasu, V.V., Sreedevi, V., Hashizume, A.,Kohmoto, H., Moehlecke, S., Ricardo R., Kopelevich, Y., Endo, T.: Physica C 362 282-285 2001.
16. Srinivasu, V.V., Thomas, B., Vasanthacharya, N Y. , Hegde, M S. Bhat, S V.: Solid State Commun. Vol 79 No9 723-716 1991.
17. Blazey, K.W., Bednorz, J.G., and Muller, K.A.: Springer Verlag, 240 1990.
18. Dulcic, A., Crepeau, R.H., and Freed, J.H.: Phys. Rev. B 38 5002 (1988).
19. Bohandy, J., Kim, B.E., Andrian, F.J., and Moorjani, K.: Phys. Rev. B 39 2733 1989.

20. Srinivasu, V.V., Thomas, B., Hedge, M.S., Bhat, S.V.: J. Appl. Phys. 75 4131-4136 1994.
21. Blazey, K.W., Muller, K.A., Bednorz, J.G., Berlinger, W., Amoretti, G., Buluggiu, E., Vera, A., and Matacotta, F.C.: Phys. Rev. B **36**, 7241 (1987).
22. Malay, R.T., and Srivastava, G.P.: IEE Transactions on magnetics, vol 35 (1999)
23. Rettori, C., Davidov, D., Belaish, I., and Felner, I.: Phys. Rev. B 36 4028 (1987).
24. Stankowski, J., Kahol, P.K., Dalai, N.S., and Moodera, J.S.: Phys. Rev. B **36,** 7128 (1987).
25. Bonvalot, M., Puri, M., and Kevan L.: J. Chem. Soc. Faraday. Trans. 88 2387 1992.
26. Gzyzak, B.: Supercond. Sci. Technol. 9 149 1996.

# Chapter 5

## Boundary Current Response in $Ba_{0.34}K_{0.64}Fe_2As_2$ Single Crystal Probed by Non-Resonant Microwave Absorption.

## 5.1 Introduction

Over the years, Non-resonant microwave absorption (NRMA) technique [1-6] has emerged as a very powerful tool to probe and study High-Tc Superconducting materials (HTSC). It was successfully used to assess the quality of superconducting thin films [7], to understand the granularity and anamolous NRMA [8], to study the boundary currents or the shielding effects [9], the manifestation of Wohlleben effect [10] to detect superconducting phases [11], to probe superconductivity at Nano scale [12], surface barrier effects [13], effect of density, magnetic Field modulation and magnetic field penetration depth [14], effects of microwave power [15], etc. Particularly low magnetic shielding or boundary current response can be probed very effectively by the NRMA technique as shown for the cuprate superconducting materials [9, 16, 17]. Mahel et al [16] describes the modulated microwave absorption in terms of the modulation of intergranular critical state and magnetization current. Dulcic et al [17] attributes the boundary current response in NRMA due to the fact that boundary current becomes modulated under the influence of the modulations field superposed on the applied dc field which is swept in the NRMA experiment. Srinivasu et al [9] have taken advantage of the model built by Dulcic et al [17] to study the magnetic shielding effects in Ag-doped YBCO thin films and showed that better grain alignment in Ag-doped YBCO thin films leads to a better shielding effect as compared to the pure YBCO thin films. It is fundamental that in a superconductor, fields smaller than $H_{c1}$ will be shielded off due to shielding or the boundary currents. Understanding these shielding effects is of importance for certain applications that involve magnetic shielding. In this context we use the NRMA technique to study the shielding or boundary current effects in $Ba_{0.34}K_{0.64}Fe_2As_2$ Single Crystals (BaK-122).

## 5.2 Experimental

The single crystal of BaK122 was synthesized through a self-flux method. The starting materials of Ba fillings (1.758g), Fe Powder (2.38g), As (3.358g) and potassium pieces (0.5g) were mixed, the procedure was carried out in a glove box with a protective Argon atmosphere in which the concentration of both $O_2$ and $H_2O$ were less than 1ppm, this mixture was then

ball milled for 9 hours, until it was homogeneous. The homogeneous mixture was put in a tube furnace at 1100$^{o}$C to melt completely. More details of the crystal growth are given elsewhere [18-20]. These crystals are phase pure and have a $T_c$ of 38K. NRMA measurements were carried out using a BRUKER EXM spectrometer operating at 9.4 GHz. Modulation field frequency was 100 KHz and the amplitude was varied between 1G to 9G. Low temperature measurements were done using an Oxford Cryostat with liquid He flow and controlling flow and heater. The single crystal was mounted on a quartz rod shaped into a flat surface at one end. Experiments were carried out in two field orientations, namely, applied field (1) parallel and (2) perpendicular to the Iron arsenide plane. The DC magnetic field was swept from -1000 G to +1000 G.

## 5.3 Results and Discussion.

The XRD patterns in Fig. 5.1 reveals that the main phase was BaK122, only the (00$\ell$) peaks with even $\ell$ are observed suggesting that the crystallographic c-axis is perpendicular to the shining surface.

Fig. 5.2 shows a resistivity versus temperature for BaK122 single crystal in zero fields. The resistivity drops at 38.2K and it vanishes at about 36.7 K which has been designated as the superconducting transition temperature $T_{C.}$

Non-resonant microwave absorption (NRMA) signal has origin essentially from two mechanisms 1. Microwave driven fluxon losses (Portis model [21]) and 2. Field reduction of Weaklinks critical currents (Dulcic model [17]). However below Hc1 the modulation field cannot push fluxons in and out and therefore only the Weaklinks modulation of the critical currents and the boundary or shielding current response shall be responsible for NRMA signals. In the scenario of Dulcic model [17], briefly described in the following:

Microwave loss depends on applied field and temperature which is then determined by the field and temperature dependence of the critical currents ($I_c$) in the Josephson Junctions.

$I_c(H,T) = I_c(0,T)F(H)$ …….(1)

T and H are temperature and field respectively. F(H) is an envelope of the reduction factor [sin(πH/Ho)/(πH/Ho)] for Ic. As a small modulation field is superposed on the applied dc field in the experiment, F(H) can then be written as $F(H + H_M \cos\omega t) = F(H) + F'(H)H_M$

$\cos\omega_M t$. Here the net boundary current ($I_b$) shall be weakly modulated as $I_b = I_c + I_M\cos\omega_M t$. $I_M$ is the modulation current due to the small modulation field and Io is the boundary current in the absence of the modulation field. Then in the limit $I_M << I_o$, one can write Dulcic's expression [17] for the microwave loss as

$$S_m = \frac{((1/2)I_{mw}^2 R)^{1/2}}{((1/2)(\hbar/2e)w_{mw})}\frac{I_C}{(1+\eta)^{3/2}}\left[-\frac{dI_C}{dH}H_M + I_M\sin\varphi\right]\cos w_M t \qquad (2)$$

The first term is a sweep-independent term and grows linearly with the modulation amplitude [17]. The second term in (2) equation changes sign due to the phase and shall give rise to the boundary current reversal response.

When $I_M << I_o$, there will be small phase oscillation around $\varphi_o$. However, when the modulating fields are high enough, in the limit $I_M \geq I_o$ the phase oscillates between positive and negative values and the boundary current response becomes negligible and the sweep independent component dominates giving rise to the derivative looking signal (in the NRMA technique, the magnetic field dependent microwave absorption is lock-in detected, giving rise to the field derivative of the microwave absorption). Thus, derivative-looking microwave absorption signals will appear when the modulating magnetic fields are high enough to suppress the boundary current effect (shielding effect). We can see this scenario in Fig.5.3 & 5.4 where NRMA signals for BaK122 crystal are plotted at various modulation fields at 30 K, when applied field is parallel and perpendicular to the superconducting Iron arsenide plane respectively.

In both the cases one can see that as the modulation field increases the NRMA signals transforms from a pure boundary current response (seen at 1 – 3 G) to a kind of mixed response of two components namely, the boundary current and flux modulated derivative response (shown with dashed circles in the figures), which is more prominent in the field perpendicular to ab-plane configuration due to the fact that now modulation field begins to push the flux in and out. Modulation field can push flux in and out when it exceeds $H_{c1}$. Another way to approach this limit is by increasing the temperature and keeping the modulation field amplitude constant. For a given modulating field, IM is constant and Io, the

boundary current can be reduced by increasing the temperature. And also $H_{c1}$ decreases as well as the temperature is increased towards $T_c$.

So in such a situation at some temperature we should begin to see the flux modulation component (derivative looking signal) as shown with dashed circles in Figs. 5.5 & 5.6 for the field parallel and perpendicular orientations with respect to the ab-plane respectively. One can see that as temperature approaches $T_c$, the derivative looking component grows, boundary current component decreases and at 32K the NRMA signal has become fully derivative like and almost the boundary current response disappeared. Further this effect is more prominent in the field orientation perpendicular to the ab-plane.

And very close to $T_c$ one would expect the suppression of the boundary current response and therefore the flux modulated component dominates which shall give rise to the derivative looking signal. This is what we observed when we measured NRMA at 32K for both field parallel and perpendicular configurations with respect to the crystal ab-plane or the Iron arsenide plane as shown in the Fig.5.7,5.8. At low temperatures far away from $T_c$ mostly boundary current response shall be dominating as shown in Fig.5.9-5.10 and Fig. 5.11-5.12. Here in this case we could not observe the flux modulation response with the highest modulation amplitude of 9G limit that we have experimentally.

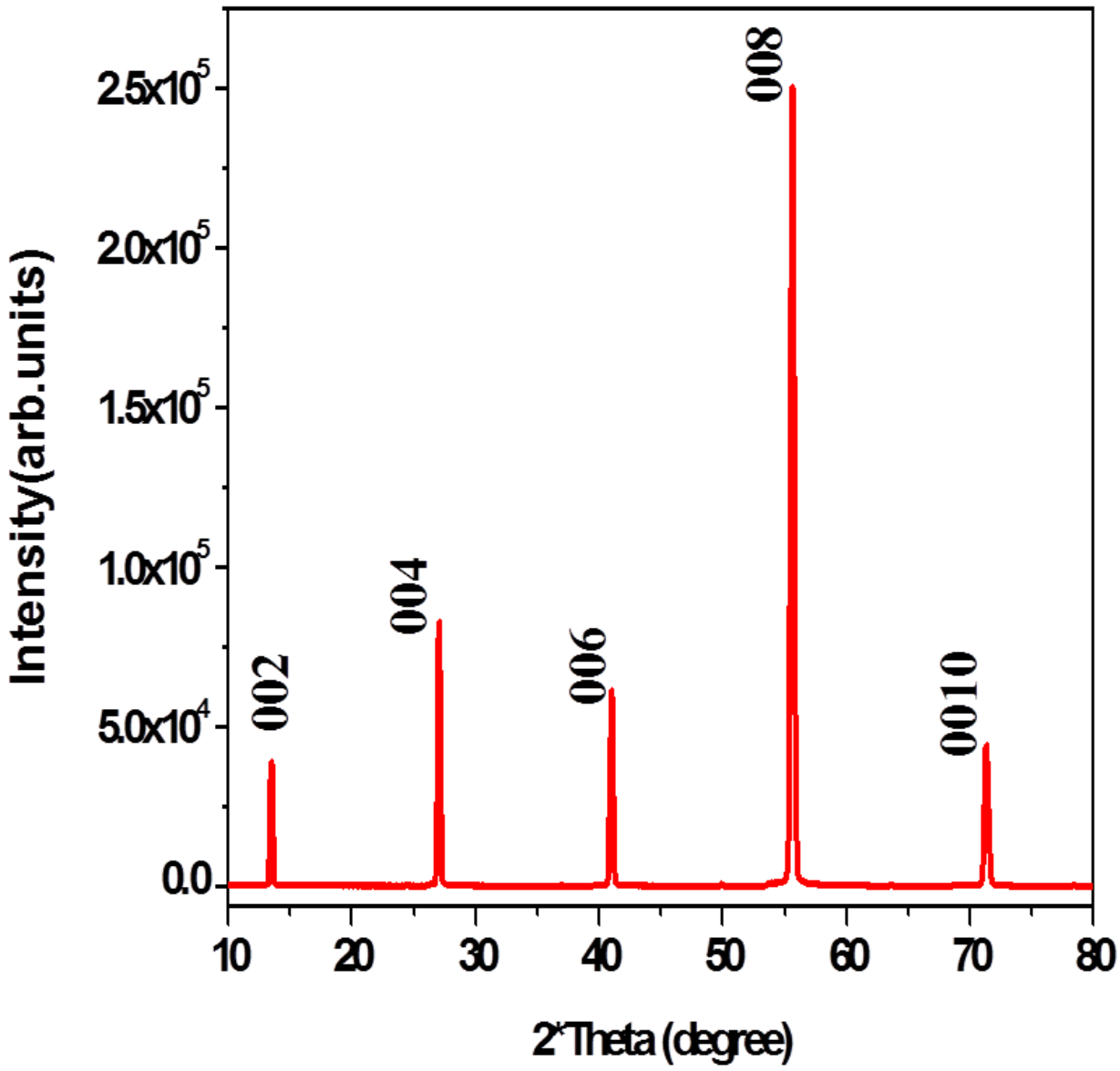


*Fig. 5.1 XRD pattern of BaK122 sample.*

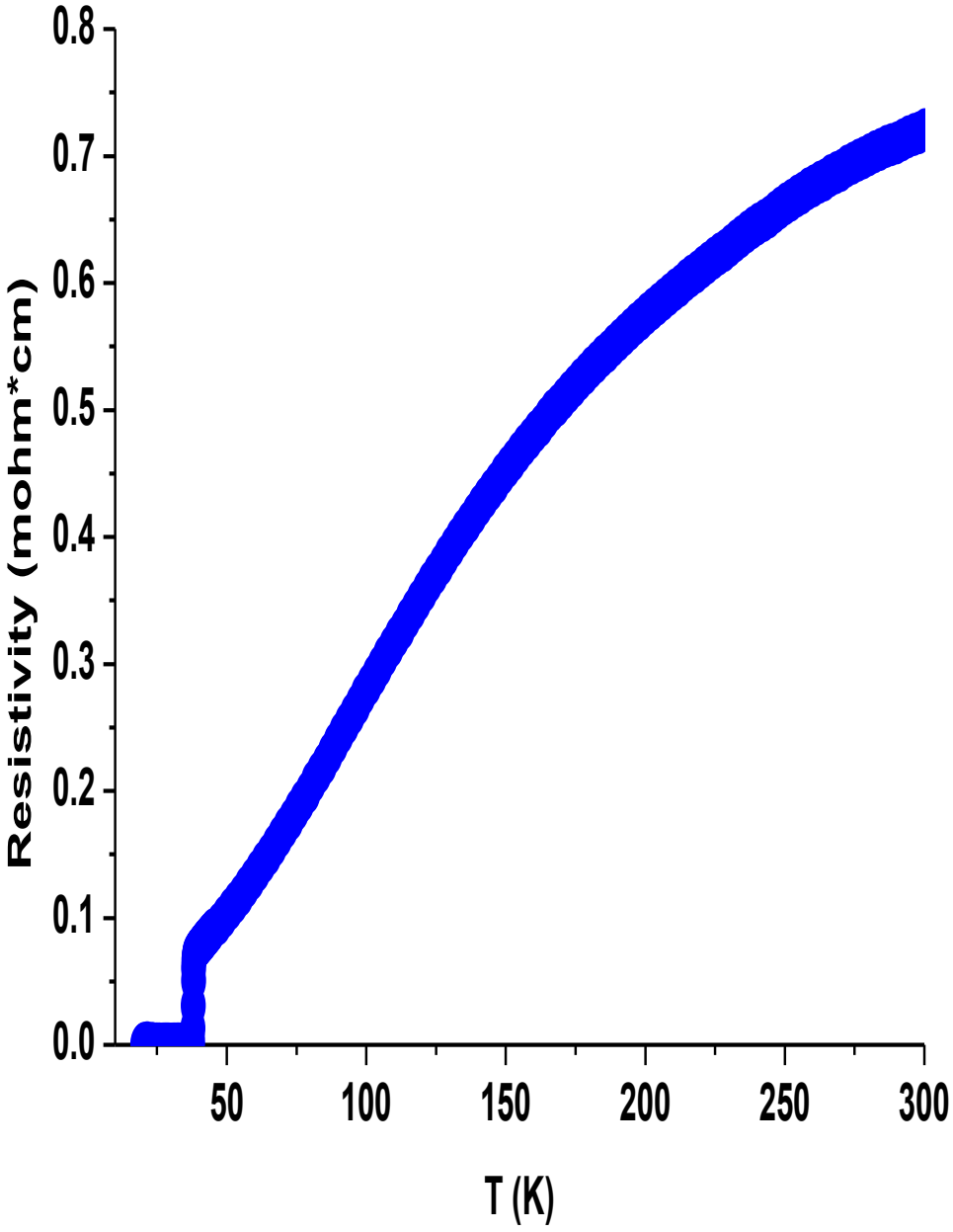


*Fig. 5.2 Temperature dependence of resistivity for BaK122 single crystal from 10K to 300K*

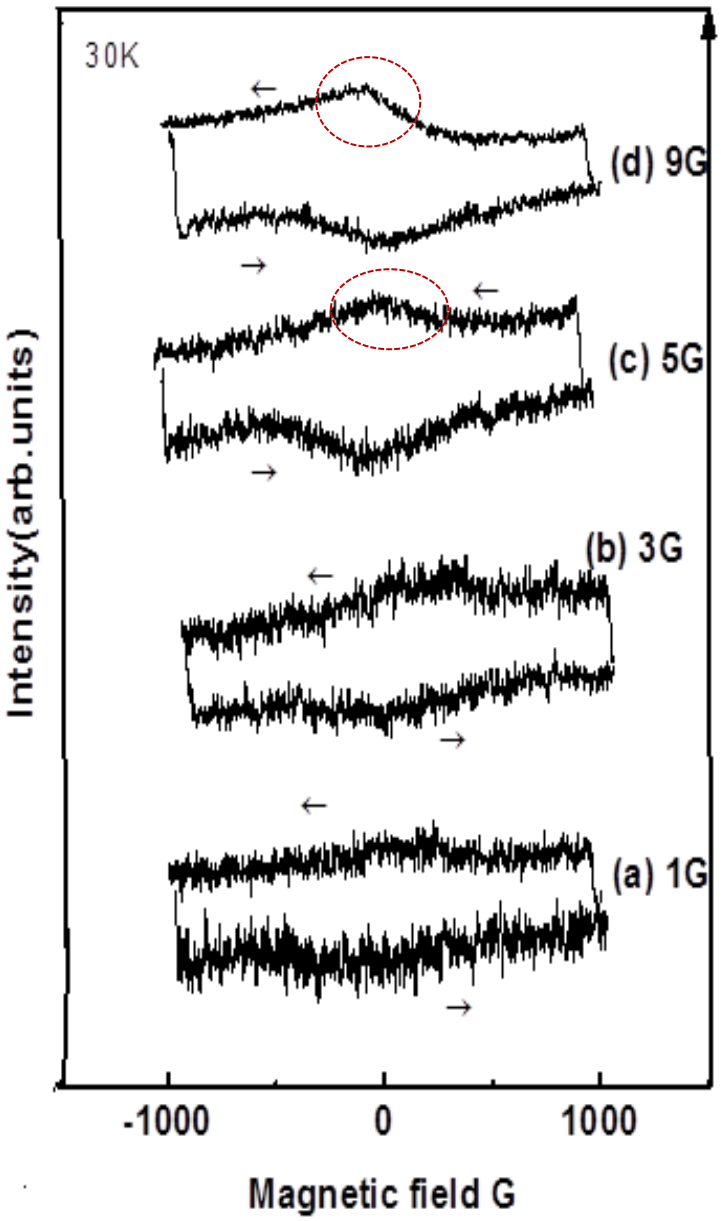


*Fig. 5.3 NRMA signal of BaK122 single crystal measured at 30 K and at various modulation field amplitudes, when the DC field is parallel to the iron arsenide plane.*

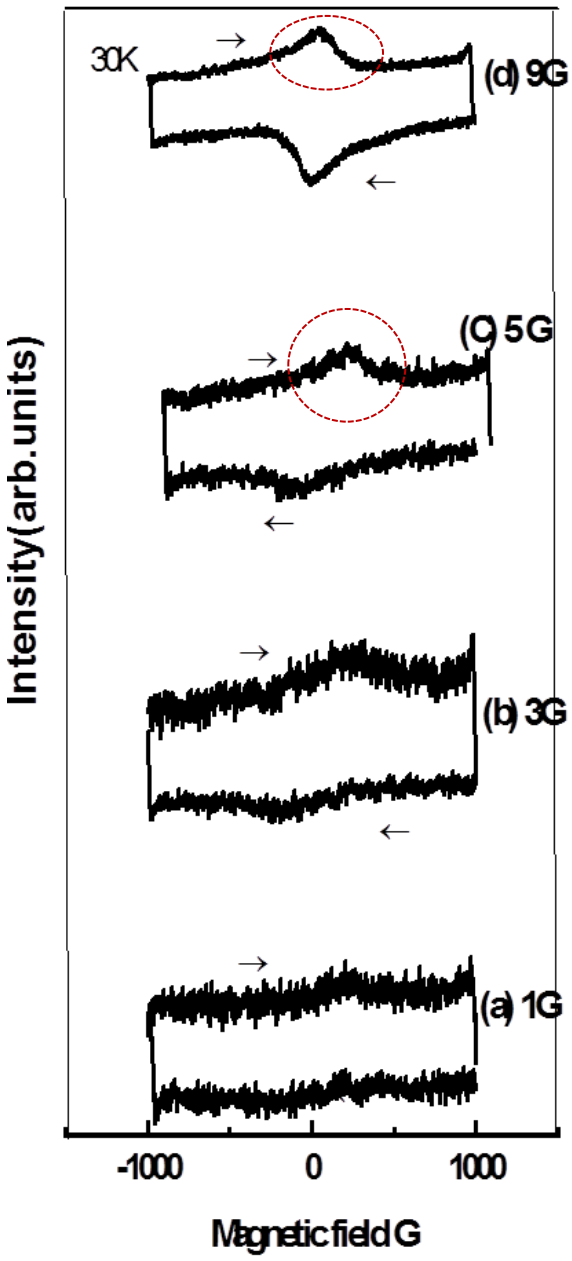


*Fig. 5.4 NRMA signals of BaK122 single crystal measured at 30 K and at various modulation field amplitudes when the DC field is applied perpendicular to the iron arsenide plane.*

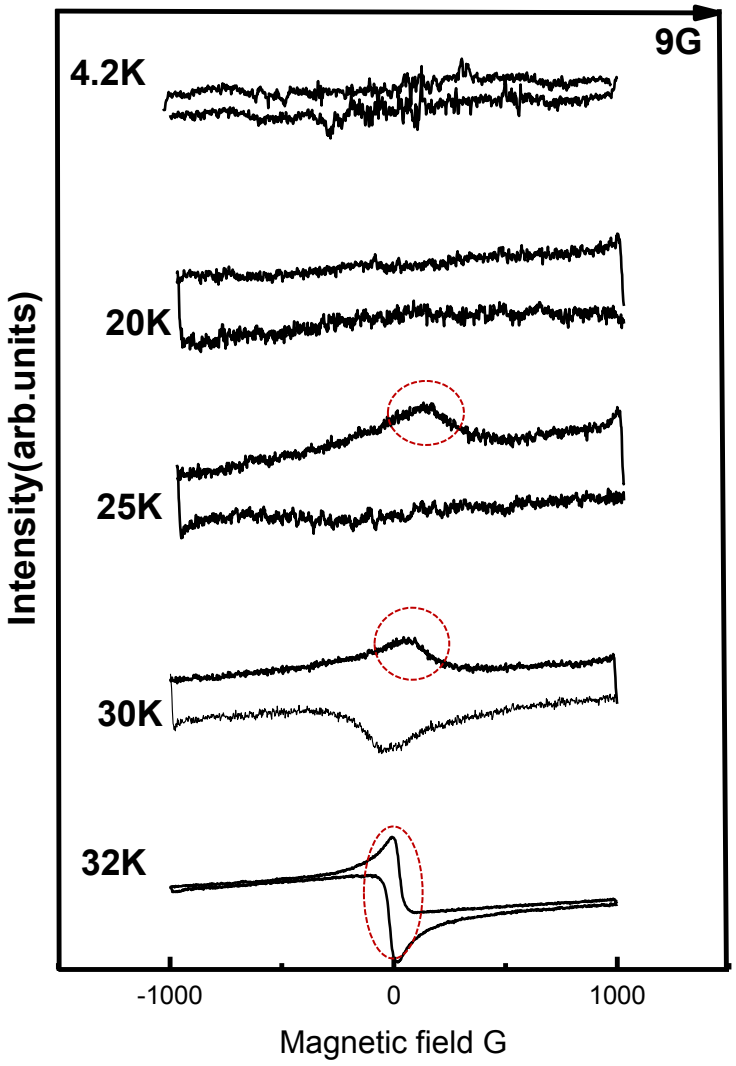


*Fig. 5.5 NRMA signals of BaK122 single crystal measured at various temperatures with a modulation field of at 9 G and the DC field is parallel to the iron arsenide plane*

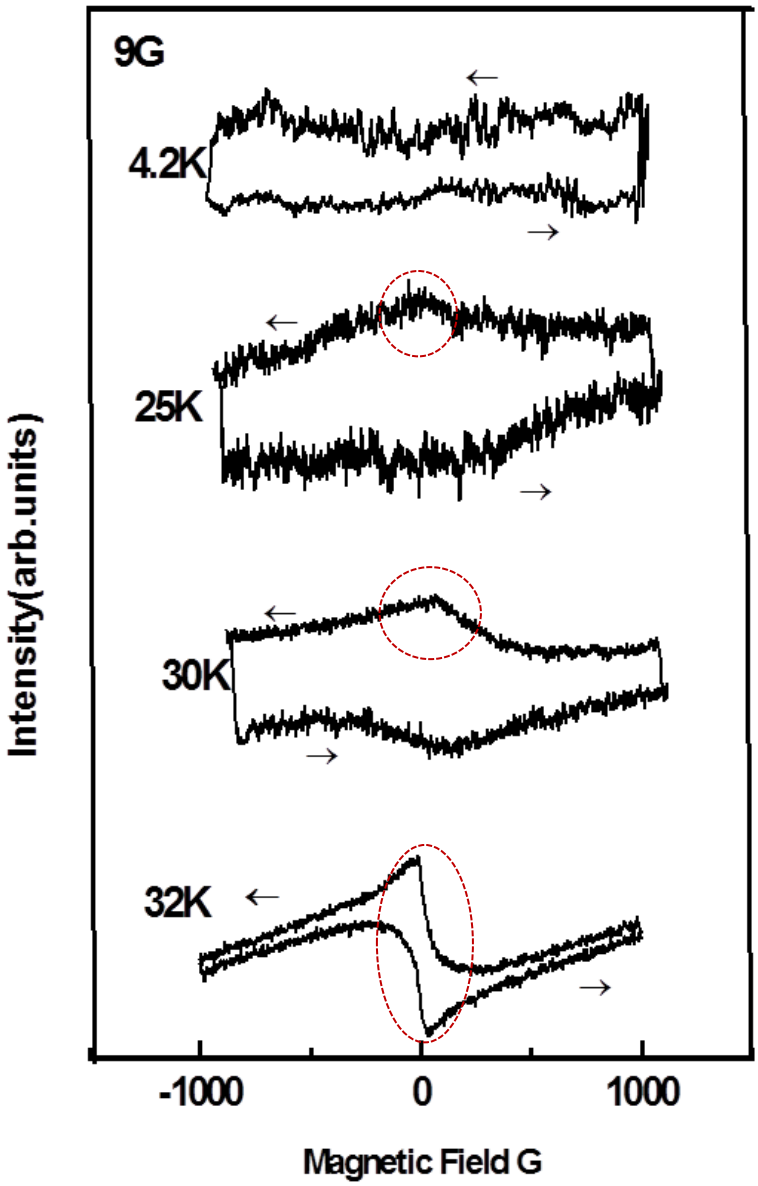


*Fig. 5.6 NRMA signals of BaK122 single crystal measured at various temperatures with a modulation field of 9 G and the DC field is perpendicular to the iron arsenide plane*

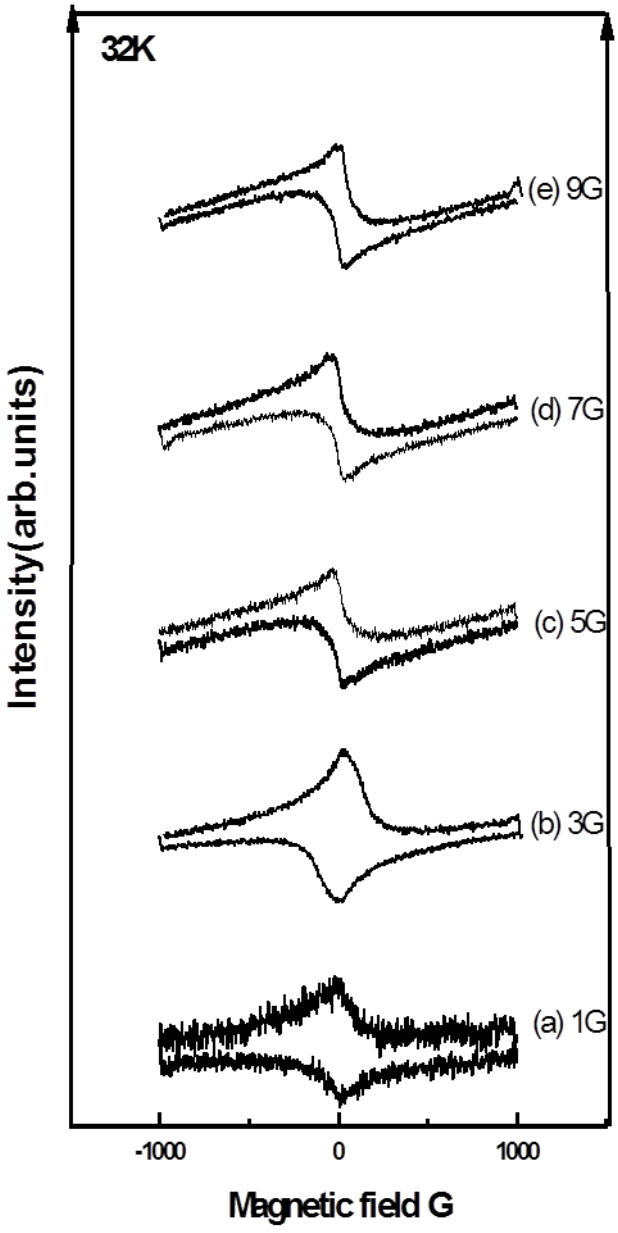


*Fig. 5.7 NRMA signals measured at 32 K at various modulation field amplitudes when the DC field is parallel to the iron*

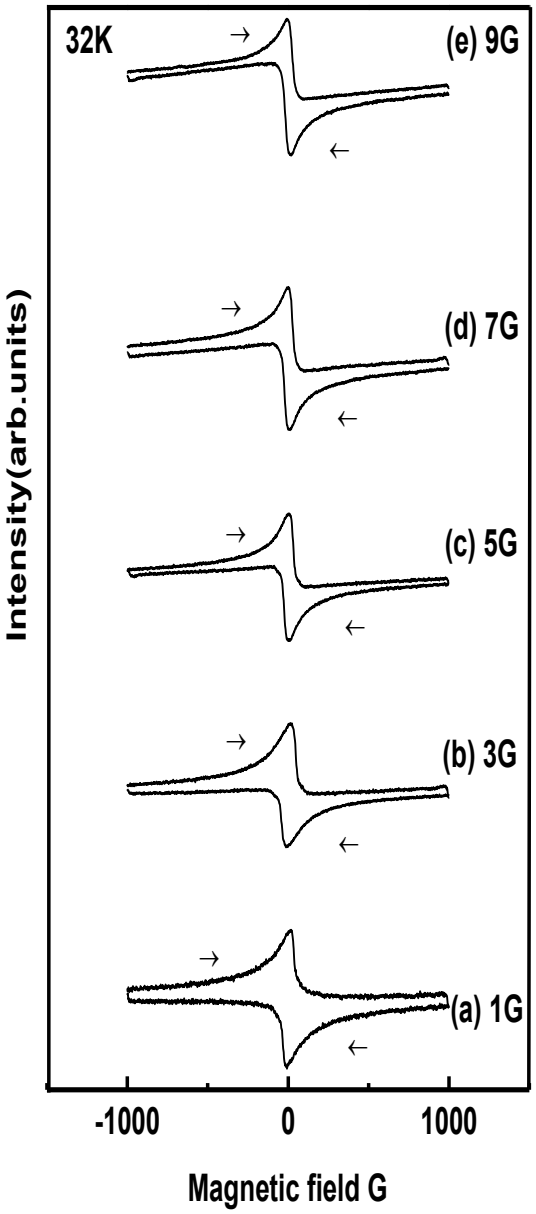


*Fig.5.8 NRMA signals of BaK122 single crystal at 32 K at various modulation field amplitudes when the field is applied perpendicular to the iron arsenide plane.*

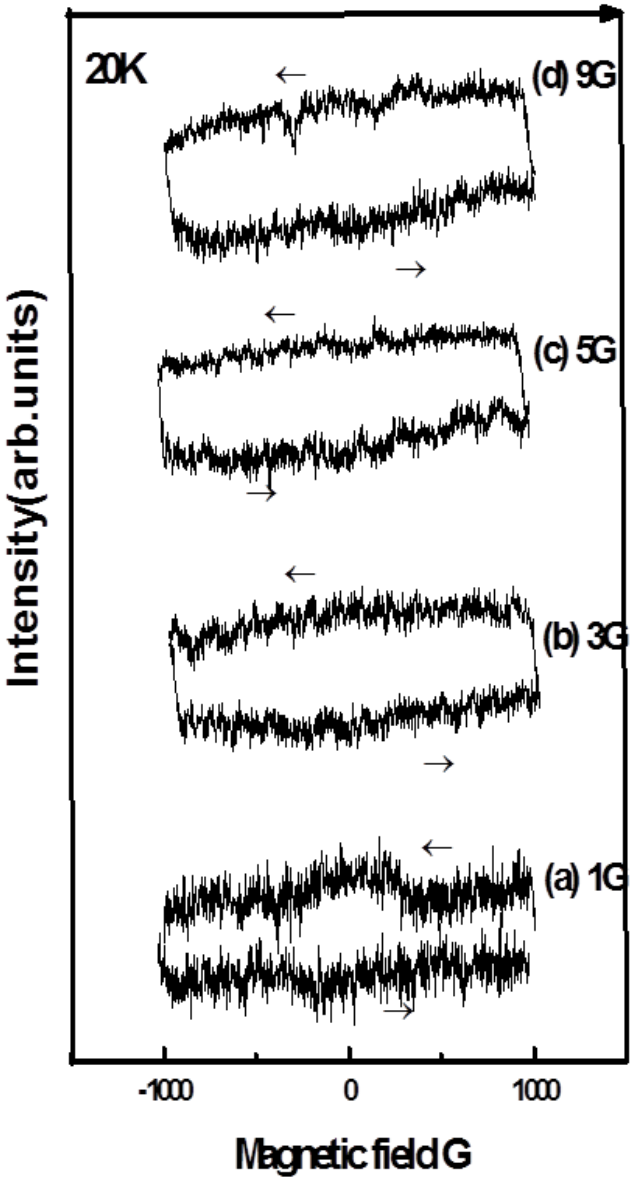


*Fig.5.9 NRMA signals at 20K measured at different modulation field with the field applied parallel the iron arsenide plane.*

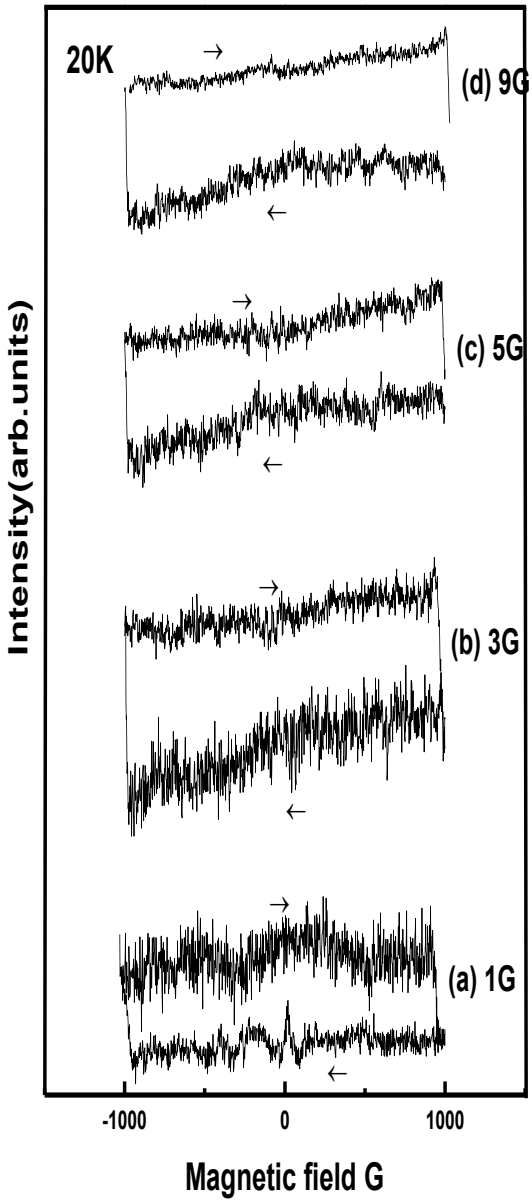


*Fig.5.10 NRMA signals at 20 K as a function of modulation field, when the DC field is applied perpendicular to the iron arsenide plane.*

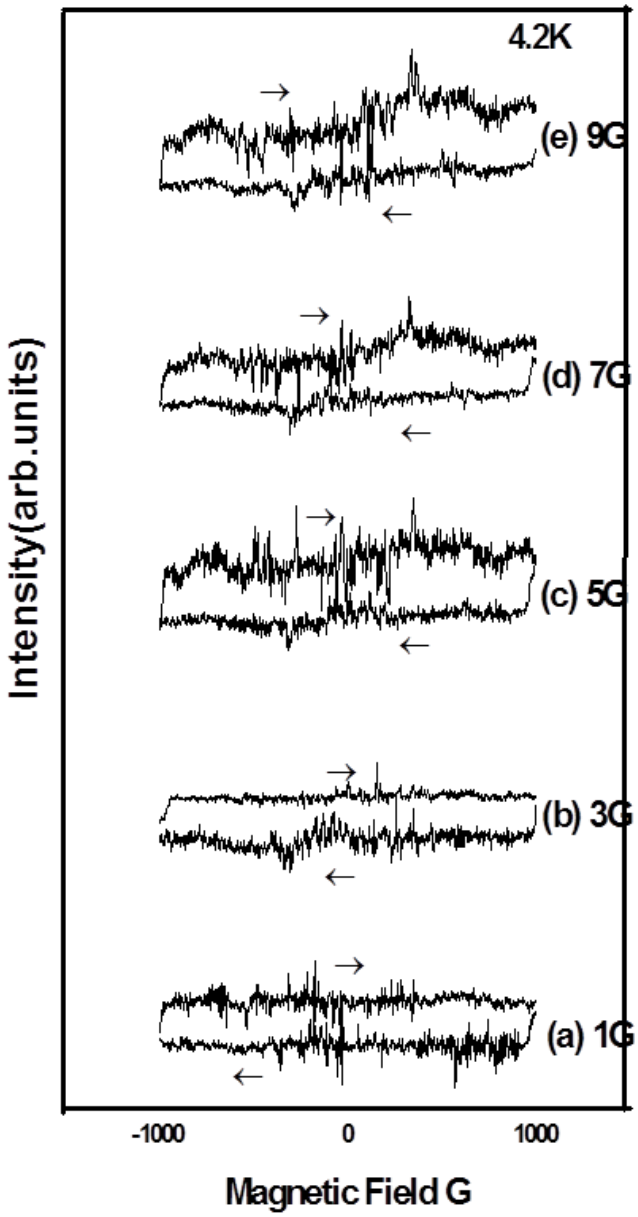


*Fig. 5.11 NRMA signals at 4.2 K as a function of modulation field, when the DC field is applied perpendicular to the iron arsenide plane*

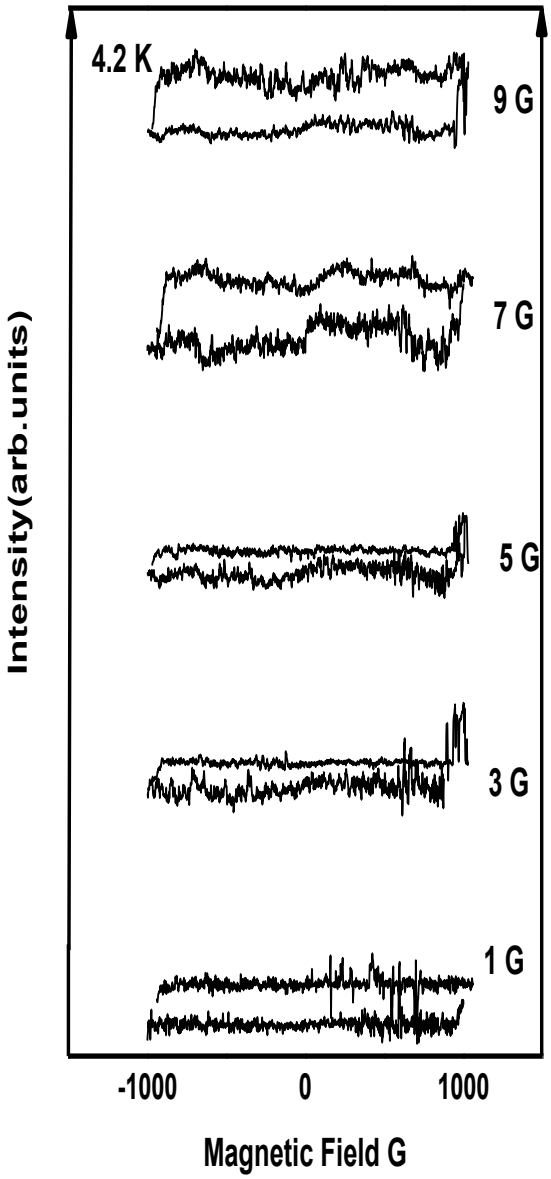


*Fig.5.12 NRMA signals at 4.2 K as a function of modulation field, when the DC field is applied parallel to the iron arsenide plane*

## 5.4 Conclusion

We have studied the boundary current or the shielding effects in BaK122 single crystals using NRMA technique at various modulation fields and temperatures below $T_c$ of the crystal. At very low modulation fields and temperatures, the NRMA signals are dominated by pure boundary current response. At intermediate temperatures and modulation fields, a mixed response with two components namely, both boundary current and flux modulation response are observed. At high temperatures close to the $T_c$ mostly a flux modulation response has been observed.

## 5.6 References


[1] Bhat, S.V., Ganguly, P., Ramakrishnan, T.V., Rao, C.N.R.:J. Phys. C 20, L559 (1987)

[2]. Blazey, K.W., Muller, K.A., Bednorz, J.G., Berlinger, W., Amoretti, G., Buluggiu, E., Vera, A., Matacotta, F.C.: Phys. Rev. B 36, 7241 (1987)

[3]. Kachaturyan, K., Weber, E.R., Tejedor, P., Stacy, A.M., Portis, A.M.: Phys. Rev. B 36, 8309 (1987)

[4]. Rettori, C., Davidov, D., Blelaish, I., Feluer, I.: Phys. Rev. B 36, 4028 (1987)

[5]. Durny, R., Hautala, J., Ducharme, S., Lee, B., Symko, O.G., Taylor, P.C., Zhang, D.J., Xu, J.A.: Phys. Rev. B 36, 2361 (1987)

[6]. Stankowski, J., Kahol, P.K., Dalal, N.S., Moodera, J.S.: Phys. Rev. B 36, 7126 (1987)

[7]. Srinivasu, V.V., Thomas, B., Hegde, M.S., Bhat, S.V.: J. Appl. Phys. 75, 4131 (1994)

[8]. Bhat, S.V., Srinivasu, V.V., Kumar, N.: Phys. Rev. B 44, 10121 (1991)

[9]. Srinivasu, V.V., Pinto, R., and Sasstry, M.D.: Applied Superconductivity Vol. 4, pp 195-201, (1996).

[10].Braunisch, W., Knauf, N., Kataev, V., Neuhausen, S., Grutz, A., Kock, A., Roden, B., Khomskii, D., and Wohlleben, D.: Phys. Rev. Lett. 68, 1908 (1992).

[11]. Khairullin, I. I., Khabibullaev P. K., Yu. V., Sokolov, A. A., Zakhidov, T.R.: J. Of Phys 23, 1107 –1126 (1999)

[12]. Shaltiel, D.; Krug von Nidda, H.A.: nanosci. and nanotechnol Lett, Vol 3, pp. 575-578(4), (2011)

[13]. Rastogi, A., Srinivasu, V.V., Hegde, M.S., Bhat, S.V.: Phys. C. Vol 234, issues 3-4, 229-231 (1994)

[14]. Puri, M., Masiakowski, J., Bear, J., and Kevan, L., J. Chem. SOC. Faraday trans., 87(22), 3687-3694 (1991).

[15]. Czyzak, B., Stankowski, J.: Atca Physica Polonica A, 99 Vol. 80 (1991).

[16]. Dulcic, A., Rakvin, B., and Pozek, M.: Europhysics. Lett. 10(6), pp. 593-598 (1989).

[17]. Mahel, M., Darula, M., and Benacka, S.: Supercon.Sci.Technol. 6 112-118 (1993).

[18]. Luo, H., Wang, Z., Yang, H., Cheng, P., Zhu, X., and Wen, H.: Supercond.Sci.Technol.21 125014 (2008).

[19]. Wang, C., Gao, Z., Yao, C., Wang, L., Qi, Y., Wang, D., Zhang, X., and Ma, Y.: Supercond. Sci. Technol. 24 065002 (2011).

[20]. Chen, G.F., Li, Z., Dong, J., Li, G., Hu, W.Z., Zhang, X.D., Song, X.H., Zheng, P., Wang, N.L., and Luo, J.L.: Physical Rev. B 78 224512 (2008).

[21]. Portis, A.M., Blazey, K.W., Muller, K.A., and Bednorz, J.G.: Euro. Phys. Lett. 5, 467 (1988).

# Chapter 6

## Conclusion and future work

## 6.1 Conclusion

Our work present the studies of NRMA of BaK122 single crystal sample at $T_c$= 38 K, we have successfully studied the boundary currents response using the Non-Resonant Microwave absorption technique. At various modulation filed (1-9 G) and temperatures (4.2- 32 K) below the $T_c$ of the sample (Bak122 single crystals), we observed the NRMA signals which were dominated by pure boundary current response, however at immediate temperatures and modulation fields, a mixed response with two components namely, both boundary current and flux modulation response are observed. At high temperatures close to the $T_c$ mostly a flux modulation response has been observed.

## 6.2 Future Works

Our future work will be to study the fundamental properties of BaK122 single crystal such as anisotropy and microwave power effect.

In addition we are going to synthesise different types of iron based superconductors i.e. thin films, polycrystalline along with the single crystals and do a comparative study of boundary currents response.

# Appendix

## A.0 Publications

1. Boundary Current Response in $Ba_{0.34}K_{0.64}Fe_2As_2$ Single Crystal Probed by Non-Resonant Microwave Absorption.